REVIEW

www.the-innovation.org

Tracking and controlling ultrafast charge and energy flow in graphene-semiconductor heterostructures

Shuai Fu,[1,2,7] Heng Zhang,[1,3,7] Klaas-Jan Tielrooij,[4,5] Mischa Bonn,[1,*] and Hai I. Wang[1,6,*]

*Correspondence: bonn@mpip-mainz.mpg.de (M.B.); h.wang5@uu.nl (H.I.W.)

Received: June 23, 2024; Accepted: December 10, 2024; Published Online: January 2, 2025; https://doi.org/10.1016/j.xinn.2024.100764

GRAPHICAL ABSTRACT

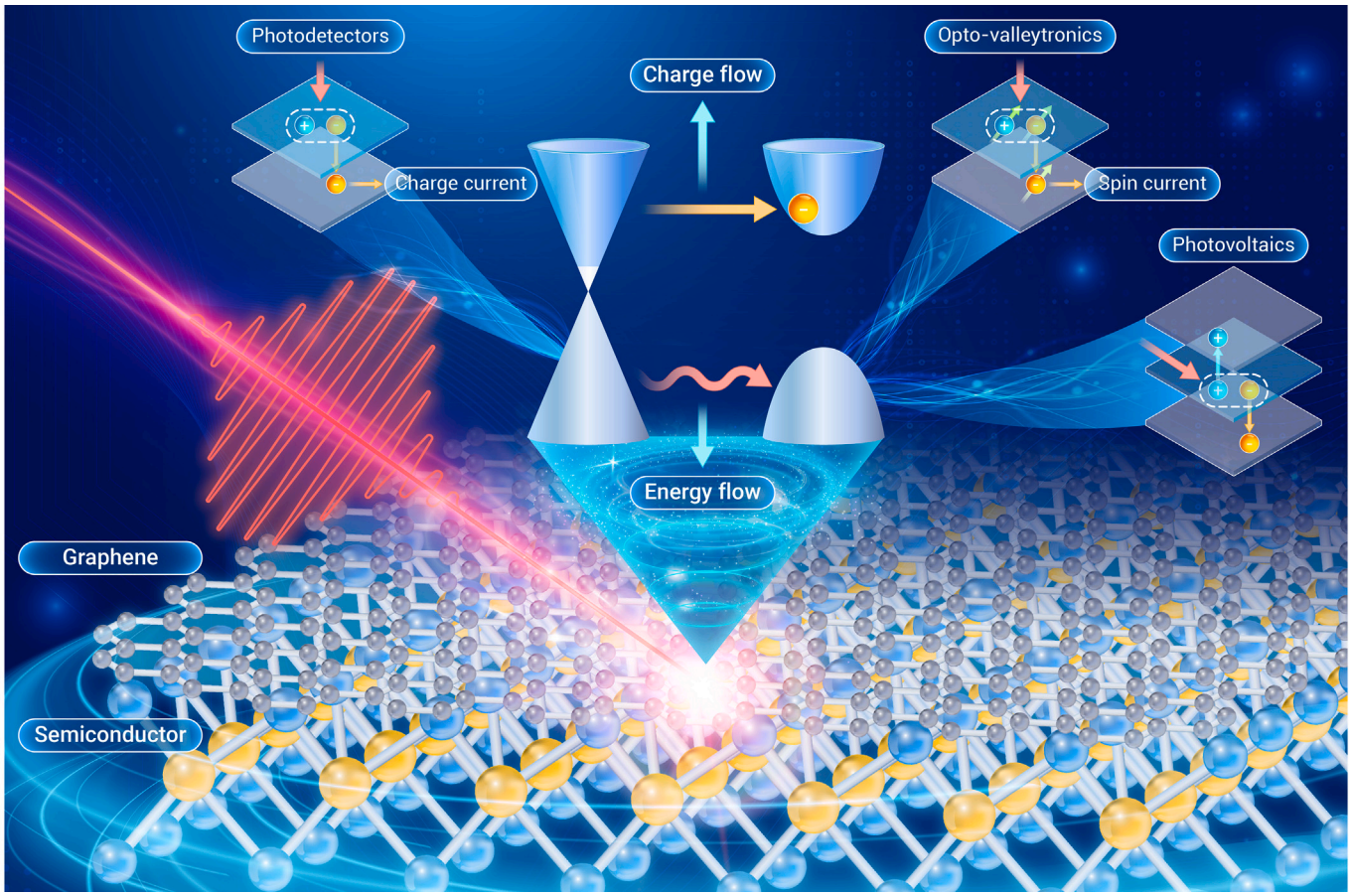

PUBLIC SUMMARY

- Review of recent developments in graphene-semiconductor heterostructures with intriguing properties.
- Summary of recent progress in interfacial charge dynamics relevant to (opto)electronic applications.
- Outlook on future research directions toward the effective control of interfacial dynamics.

OPEN ACCESS

REVIEW

The Innovation

Tracking and controlling ultrafast charge and energy flow in graphene-semiconductor heterostructures

Shuai Fu,[1,2,7] Heng Zhang,[1,3,7] Klaas-Jan Tielrooij,[4,5] Mischa Bonn,[1,*] and Hai I. Wang[1,6,*]

[1]Max Planck Institute for Polymer Research, 55128 Mainz, Germany

[2]Center for Advancing Electronics Dresden (cfaed) and Faculty of Chemistry and Food Chemistry, Technische Universität Dresden, 01062 Dresden, Germany

[3]Department of Physics, University of Regensburg, 93040 Regensburg, Germany

[4]Catalan Institute of Nanoscience and Nanotechnology (ICN2), BIST and CSIC, Campus UAB, 08193 Bellaterra (Barcelona), Spain

[5]Department of Applied Physics, TU Eindhoven, 5612 AZ Eindhoven, the Netherlands

[6]Nanophotonics, Debye Institute for Nanomaterials Research, Utrecht University, 3584 CC Utrecht, the Netherlands

[7]These authors contributed equally

*Correspondence: bonn@mpip-mainz.mpg.de (M.B.); h.wang5@uu.nl (H.I.W.)

Received: June 23, 2024; Accepted: December 10, 2024; Published Online: January 2, 2025; https://doi.org/10.1016/j.xinn.2024.100764

Citation: Fu S., Zhang H., Tielrooij K.-J., et al., (2025). Tracking and controlling ultrafast charge and energy flow in graphene-semiconductor heterostructures. The Innovation **6(3)**, 100764.

Low-dimensional materials have left a mark on modern materials science, creating new opportunities for next-generation optoelectronic applications. Integrating disparate nanoscale building blocks into heterostructures offers the possibility of combining the advantageous features of individual components and exploring the properties arising from their interactions and atomic-scale proximity. The sensitization of graphene using semiconductors provides a highly promising platform for advancing optoelectronic applications through various hybrid systems. A critical aspect of achieving superior performance lies in understanding and controlling the fate of photogenerated charge carriers, including generation, transfer, separation, and recombination. Here, we review recent advances in understanding charge carrier dynamics in graphene-semiconductor heterostructures by ultrafast laser spectroscopies. First, we present a comprehensive overview of graphene-based heterostructures and their state-of-the-art optoelectronic applications. This is succeeded by an introduction to the theoretical frameworks that elucidate the fundamental principles and determinants influencing charge transfer and energy transfer—two critical interfacial processes that are vital for both fundamental research and device performance. We then outline recent efforts aimed at investigating ultrafast charge/energy flow in graphene-semiconductor heterostructures, focusing on illustrating the trajectories, directions, and mechanisms of transfer and recombination processes. Subsequently, we discuss effective control knobs that allow fine-tuning of these processes. Finally, we address the challenges and prospects for further investigation in this field.

INTRODUCTION

A wealth of low-dimensional materials with fascinating optical and electrical properties—often beyond the reach of their bulk counterparts—has significantly expanded the candidate library for next-generation optoelectronic applications. One of the most prominent examples is the mechanical exfoliation of graphene, which consists of a monolayer of sp^2-hybridized carbon atoms arranged in a honeycomb lattice.[1] The massless nature of charge carriers in graphene renders it one of the most conductive materials ever discovered, with reported charge mobilities exceeding 100,000 $cm^2/(V\cdot s)$.[2–4] Furthermore, owing to its gapless electronic band structure, graphene exhibits ultra-broadband electromagnetic absorption covering frequencies from ultraviolet to terahertz.[5–8] The combination of ultrahigh charge mobility and broadband optical absorption makes graphene highly promising for light sensors and detectors.[9] Despite the success of several proof-of-concept demonstrations, photodetectors with graphene as the photoactive material typically have a responsivity well below 1 A/W.[10–16] Such low responsivity is primarily attributed to graphene's relatively weak optical absorption (2.3% for suspended graphene)[7,8] and, in the case of hot-carrier-based detectors,[17] the short photocarrier lifetime, which is on the order of a few picoseconds (ps).[18–22] In this context, enhancing graphene's light detection sensitivity through the incorporation of other low-dimensional building blocks that exhibit strong light-matter interactions presents a promising route, as it can simultaneously increase optical absorption and extend excited-state lifetimes through interfacial charge separation.[23,24] Furthermore, the tunable dimensionality, thickness, and chemical composition of sensitizers, along with designable interlayer electronic coupling and programmable stacking configurations, provide a versatile toolkit for pursuing high-performance photodetectors. For example, Konstantatos and Koppens et al.[24] pioneered the integration of zero-dimensional (0D) colloidal quantum dots (QDs) on graphene to create mixed-dimensional van der Waals heterostructures (vdWHs). The resulting phototransistor exhibited an ultrahigh photodetection gain of $\sim 10^8$ electrons per photon and a responsivity of $\sim 10^7$ A/W. Following this seminal work, the types of sensitizers have been substantially expanded (Figure 1), leading to numerous photodetectors with broad bandwidth and exceptional properties.[9,24,31–33]

Beyond photodetection, graphene-semiconductor vdWHs also offer numerous possibilities for advancing emerging optoelectronic applications,[34] including but not limited to photovoltaics,[35–38] opto-valleytronics,[28,39] photocatalysis,[40,41] modulators,[42,43] and photoresponsive memory devices (Figure 1).[44] For instance, thanks to its excellent in-plane mechanical strength, ease of solution processability, outstanding charge carrier mobility, and high optical transparency, graphene can function as a transparent electrode or an atomically thin photoabsorber in photovoltaic cells. In 2010, Li et al.[45] demonstrated the first graphene-on-silicon Schottky junction solar cell, achieving a power conversion efficiency (PCE) of 1.5% under AM 1.5G irradiation. Subsequent research has focused on improving efficiency and robustness through several approaches: (1) tuning graphene's work function through chemical doping,[46] (2) boosting light absorption and current density by leveraging the plasmonic effects of metallic nanoparticles anchored on graphene,[47,48] (3) implementing antireflection coatings,[49] (4) augmenting the surface-junction barrier and open-circuit voltage by incorporating electron-blocking and/or hole-transporting interlayers to reduce carrier recombination,[50–54] and (5) interfacing graphene with other promising photovoltaic materials, such as III–V family compounds and hybrid perovskites.[55–59] These strategies have enabled graphene-semiconductor-based solar cells to achieve remarkable PCE values exceeding 18%.[60,61]

In the field of photocatalysis, graphene-semiconductor vdWHs have been widely employed in heterogeneous photocatalytic applications, including photocatalytic water splitting, pollutant degradation, carbon dioxide reduction, and bacterial disinfection.[62] In these contexts, the graphene-semiconductor interface is expected to reduce the charge recombination rate through facilitating interfacial charge separation, thereby enhancing the overall photocatalytic efficiency. For example, Sorcar et al.[27] synthesized Pt-sensitized graphene-titania heterostructures for carbon dioxide reduction. Their findings indicated that efficient interfacial charge separation occurs upon light absorption, with photogenerated holes and electrons accumulating in graphene and on the Ti^{3+} sites, respectively, contributing to a high combined photocatalytic yield of ethane and methane of 7.9%.

Graphene-semiconductor vdWHs also hold significant opportunities in opto-valleytronics, which exploits electron spin and valley degrees of freedom for information storage and logic operations. A prominent material architecture involves vdWHs composed of graphene and transition metal dichalcogenides (TMDCs), where the strong light-matter interactions and spin-valley locking in TMDCs complement graphene's exceptional electron and spin transport properties. Luo et al.[39] performed in-plane Hanle spin precession measurements in monolayer MoS_2/few-layer graphene vdWHs, marking the first experimental observation of room temperature opto-valleytronic spin injection from MoS_2 to few-layer graphene. This was followed by lateral spin transport within the few-layer graphene

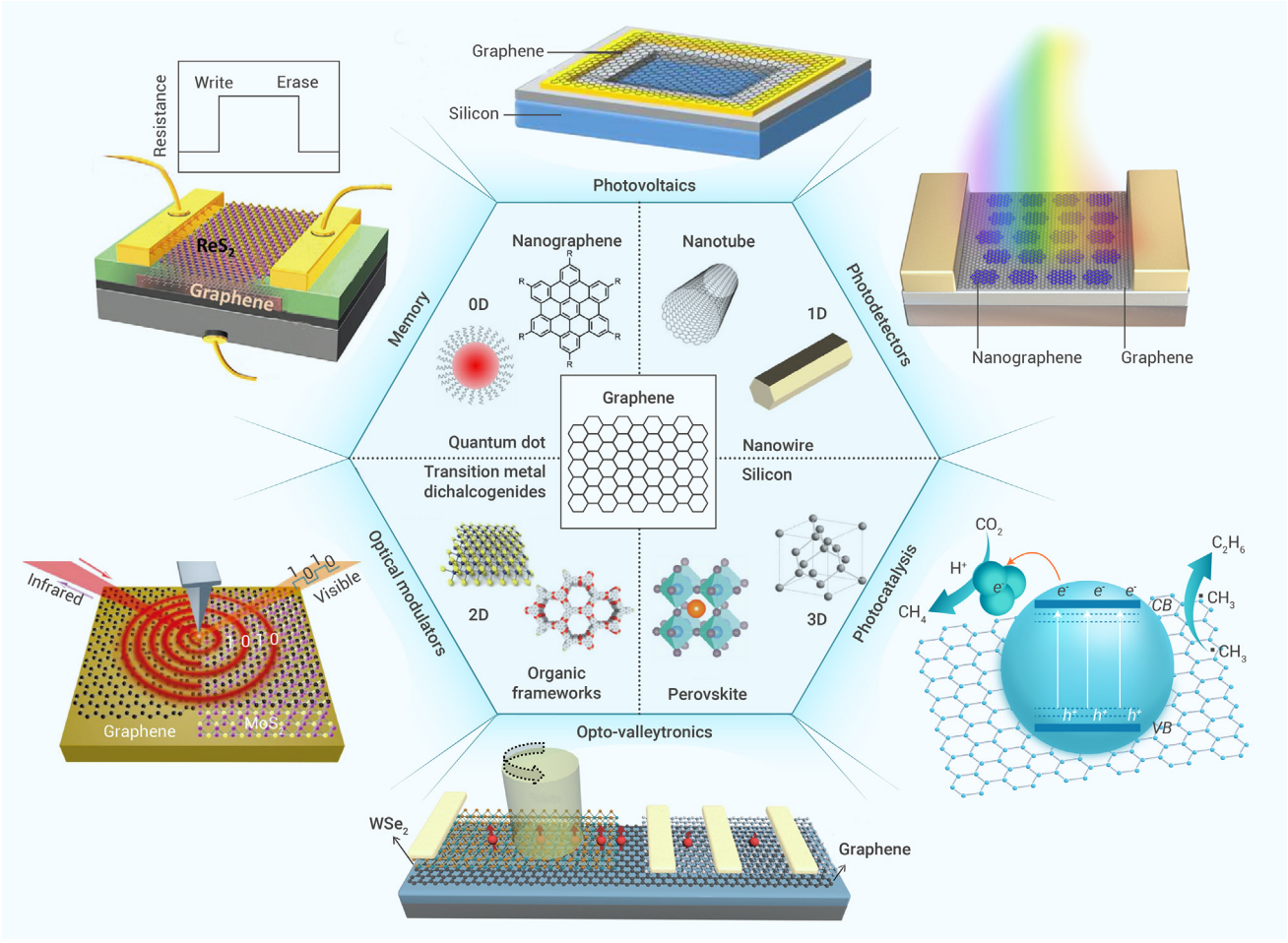

Figure 1. Graphene-based vdWHs and their (opto)electronic applications Figures reproduced with permission: photovoltaics, Miao et al.,[25] copyright 2012, American Chemical Society; photodetectors, Liu et al.,[26] copyright 2021, American Chemical Society; photocatalysis, Sorcar et al.,[27] copyright 2018, The Royal Society of Chemistry; opto-valleytronics, Avsar et al.,[28] copyright 2017, American Chemical Society; optical modulators, Guo et al.,[29] copyright 2020, Wiley-VCH; memory, Mukherjee et al.,[30] copyright 2020, Wiley-VCH.

layer and electrical spin detection using a ferromagnetic (FM) spin detector with in-plane magnetization. Avsar et al.[28] further designed vdWHs comprising monolayer WSe_2, monolayer graphene, and hexagonal boron nitride (*h*-BN) for efficient spin injection. This architectural design benefited from a near-unity valley polarization, high external quantum efficiency, and strong spin-orbit-coupling-induced spin splitting of up to ~450 meV of monolayer WSe_2.[63] They discovered that circularly polarized light stimulated spin-polarized charge carriers in the WSe_2 layer through spin-coupled valley-selective absorption. The resulting spin-polarized charges could be injected into the adjacent graphene layer and then migrate up to 3.5 μm to Co/*h*-BN contacts. The advanced tunability of the spin polarization magnitude and direction via helicity, photon energy, and material composition paved the way for versatile 2D spintronic devices for memory and logic applications.[30]

Furthermore, integrating graphene with optical waveguides has led to advancements in the development of optical modulators, where the coupling between evanescent waves and graphene can be greatly enhanced to increase the interaction length. In 2011, Liu et al.[64] reported the first waveguide-integrated graphene-based electro-absorption modulator by integrating graphene with a Si waveguide. By electrically tuning graphene's Fermi level (E_F), they achieved an optical modulator featuring a broad optical bandwidth (1.35–1.60 μm), a compact device footprint (25 μm^2), and a high operation speed (1.2 GHz at 3 dB) under ambient conditions. Subsequent development by Phare et al.[65] led to the realization of an ultrafast graphene-based modulator that effectively overcame the trade-off between speed and efficiency by exploiting critical coupling effects in a silicon nitride ring resonator, achieving an operation bandwidth of 30 GHz and a modulation efficiency of 15 dB per 10 V. Recent efforts toward on-chip all-optical devices have scaled down the building blocks to the 2D limit by employing graphene-TMDC vdWHs. Thanks to the ultrafast charge injection from monolayer MoS_2 to graphene, Guo et al.[29] achieved plasmonic modulation of 44 cm^{-1} under light-emitting diode (LED) light with an intensity as low as 0.15 mW/cm^2, which is four orders of magnitude smaller than that of conventional graphene-based, nonlinear, all-optical modulators ($\approx 10^3$ mW/cm^2). These findings establish a foundation for ultracompact on-chip optical modulators with low energy consumption, which could be crucial for next-generation information processing and communication.

From a microscopic perspective, the device performance of such heterostructures is often intricately connected to the interface physics. Therefore, understanding and controlling interfacial charge carrier dynamics is crucial for optimizing device performance. Recent studies[23,26,66–83] have investigated photo-induced charge/energy flow in various graphene-based vdWHs. We direct the reader to previous references,[84,85] where the fundamentals of charge transfer (CT) and energy transfer (ET) phenomena in vdWHs have been extensively discussed. Yet, to the best of our knowledge, timely reviews elucidating the detailed interfacial processes, the competing nature of CT and ET, and their control knobs are still lacking. To fill this gap, this review summarizes recent advances and debates in tracking and controlling interfacial CT/ET and recombination in graphene-semiconductor vdWHs. We first focus on the physical processes and dynamical phenomena taking place at graphene-semiconductor interfaces. Following this, we further introduce the mechanisms controlling the flow of charge and energy at these interfaces and how the rates can be tuned externally. Finally, challenges and opportunities in this field are discussed to guide further research.

UNDERSTANDING ULTRAFAST CHARGE AND ENERGY FLOW ACROSS GRAPHENE-SEMICONDUCTOR vdW INTERFACES

Fundamentals of CT and ET processes

CT and ET processes are ubiquitous and crucial for a wide range of technological applications, including biosensing, photosynthesis, photocatalysis,

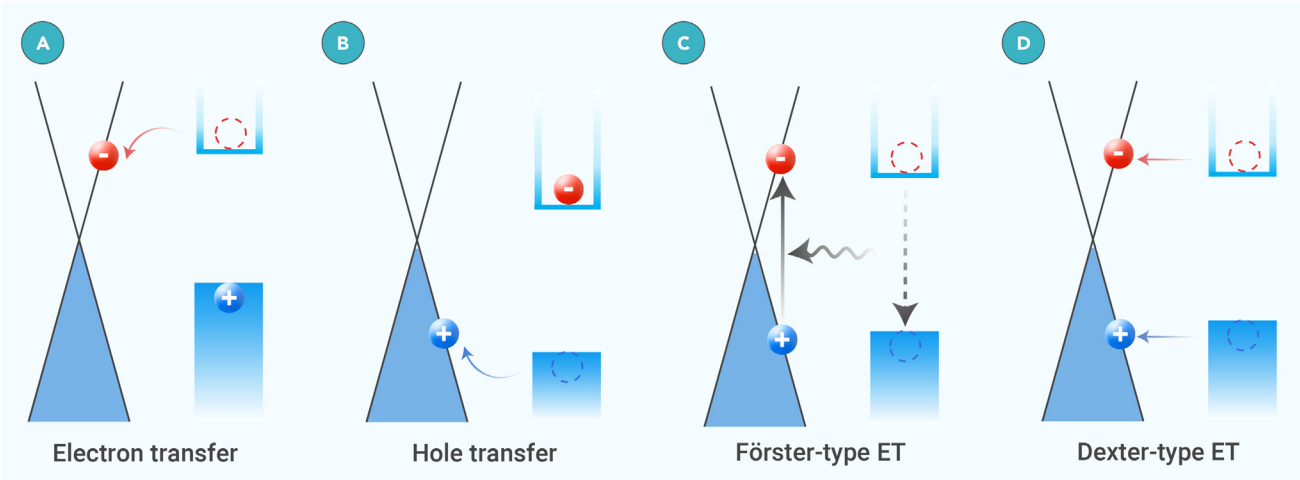

Figure 2. Schematics of CT and ET pathways (A and B) Photo-induced (A) electron transfer and (B) hole transfer. (C and D) Photo-induced (C) Förster-type and (D) Dexter-type ET. As examples, here we consider the semiconductor as the donor and graphene as the acceptor.

photovoltaics, and photodetection.[84,86–88] Graphene-based vdWHs provide an exceptional platform for exploring CT/ET, thanks to the dangling-bond-free atomic interface without any lattice matching constraints and the ultimate proximity that facilitates near-field electronic coupling.

Upon photon absorption in a semiconductor, photogenerated charge carriers can undergo relaxation and transfer phenomena involving CT/ET across the interface. The interfacial relaxation process can generally be divided into CT (via, e.g., electron or hole transfer), Förster-type ET, and Dexter-type ET (Figures 2A–2D).

Among them, CT is a short-range process (within 1 nm) that leads to the buildup of net charges of opposite signs in adjacent layers.[85] In contrast, Förster- and Dexter-type ET are non-radiative processes with no net charge accumulation on either side of the constituent. Specifically, Förster-type ET is a relatively long-range process (1–10 nm) mediated by near-field dipole-dipole coupling, in which the acceptor instantly absorbs virtual photons emitted from the donor. The Förster-type ET rate (k_{FET}) depends on the donor-acceptor distance, their spectral overlap, and the relative orientation of their dipole moments. Previous studies have shown that k_{FET} is inversely proportional to the donor-acceptor distance, with a power-law exponent determined by the geometry and dimension of the acceptor.[89–91] In contrast, Dexter-type ET relies on wavefunction overlap between the donor and acceptor and occurs in the form of short-range coulomb interactions (<1 nm) by simultaneously transferring photogenerated electrons and holes from the donor to the acceptor. This feature allows Dexter-type ET to occur even between two non-emissive electronic states in a manner that obeys Wigner's spin conservation rules (e.g., ET between two spin-allowed singlet states or two spin-forbidden triplet states).[92] Along with Förster-type and Dexter-type ET mechanisms, it is worth highlighting that near-field radiation also enables efficient energy flow across the graphene interface. This includes processes such as the cooling of hot carriers in graphene to substrate phonons via electron-hyperbolic phonon coupling[93] and plasmon launching into graphene from nearby quantum emitters.[94]

These theoretical considerations suggest that CT/ET rates and efficiencies are susceptible to both intrinsic factors, such as electronic coupling strength, driving force, and Fermi energy, and extrinsic factors, including the environment and temperature. From this aspect, graphene-based vdWHs offer tremendous opportunities to exploit the subtle interplay between these determinants through rational design of the chemical composition, dimensionality, stacking configuration, defect, dielectric environment, etc. Furthermore, considering the unique band alignment of graphene-semiconductor vdWHs, CT and ET can coexist with efficiencies determined by their rate competition. Both processes have profound implications for optoelectronic applications. For instance, CT at the graphene-WS_2 interface has been shown to induce long-lived charge separation and produce the so-called photogating effect to modulate the channel conductance,[9,23,95] thereby contributing to the ultrahigh photoconductive gain and responsivity of photodetectors.[96–98] Furthermore, Förster-type ET from nitrogen-vacancy centers in diamond to graphene has been demonstrated to generate extra electron-hole pairs in graphene, whose electrical readout, in turn, allows detection of the excited state and spin information of the optical emitter, relevant for quantum technologies and metrology.[99]

CT and ET: Experimental observations unveiling interfacial relaxation pathways

Recent developments in laser spectroscopy and microscopy provide noninvasive and quantitative approaches to studying interfacial charge carrier dynamics with ultimate temporal and spatial resolution.

Time- and angle-resolved photoemission spectroscopy (tr-ARPES) is a powerful tool that directly maps time-, energy-, and momentum-resolved charge carrier dynamics.[68,79–81,83,100] For example, Aeschlimann et al.[68] employed tr-ARPES to investigate photo-induced non-equilibrium processes in epitaxial graphene-WS_2 vdWHs (Figure 3A). Following resonant photoexcitations, they tracked photoelectron gain and loss in different energy-momentum regions (Figure 3B). They found that the WS_2 conduction band was populated with electrons undergoing single-exponential decay with a lifetime of 1.1 ps. In contrast, no hole population was detected in the WS_2 valence band (Figure 3C). On the graphene side, the electron gain above the equilibrium chemical potential decayed much faster (180 fs) than the electron loss below the equilibrium chemical potential (1.8 ps). Altogether, these observations suggested that photogenerated holes in WS_2 are rapidly transferred to graphene within the instrument response, while photogenerated electrons remain in the WS_2 conduction band, resulting in a charge separation lifetime of ~1 ps. The net density of photogenerated holes transferred from WS_2 to graphene was estimated to be $\sim 5 \times 10^{12}$ cm^{-2} (Figure 3D).

Combining tr-ARPES and microscopic many-particle theory, follow-up studies[81,83] by the same group further revealed that the CT mechanism strongly depends on the pump fluence. As shown in Figure 3E, with an increase of the pump fluence, (1) the hole transfer rate from WS_2 to graphene increases, (2) the lifetimes of photogenerated electrons in the WS_2 conduction band decrease, and (3) the lifetime of the charge-separated state increases. The observed asymmetric electron and hole transfer rates and their pump-fluence dependence were explained by direct tunneling at the band crossing of graphene and WS_2 (Figure 3F). The authors rationalized the smaller tunneling energy barrier and larger tunneling matrix elements for the holes in WS_2 compared to the electrons by a scenario in which hole transfer is more favorable than electron transfer. However, it was also noted that direct tunneling alone fails to reproduce the longer lifetime of the charge-separated state at higher pump fluences, suggesting other competing CT channels (e.g., defect-assisted tunneling channels; Figure 3F) coexist. Overall, these results provide compelling evidence for CT and its trajectories in graphene-based vdWHs.

Along with CT, ET is another important interfacial relaxation channel. In particular, even for the same above-mentioned graphene-WS_2 heterostructure, Ferrante et al.[101] reported efficient ET using time-resolved Raman scattering spectroscopy. ET was apparent from pump-induced transient changes in the G mode and 2D mode in graphene, both of which are sensitive to doping and electronic temperature (T_e) induced by external perturbations.[102–106] CT causes transient changes in the E_F and T_e, manifested by the evolution of the line shape and

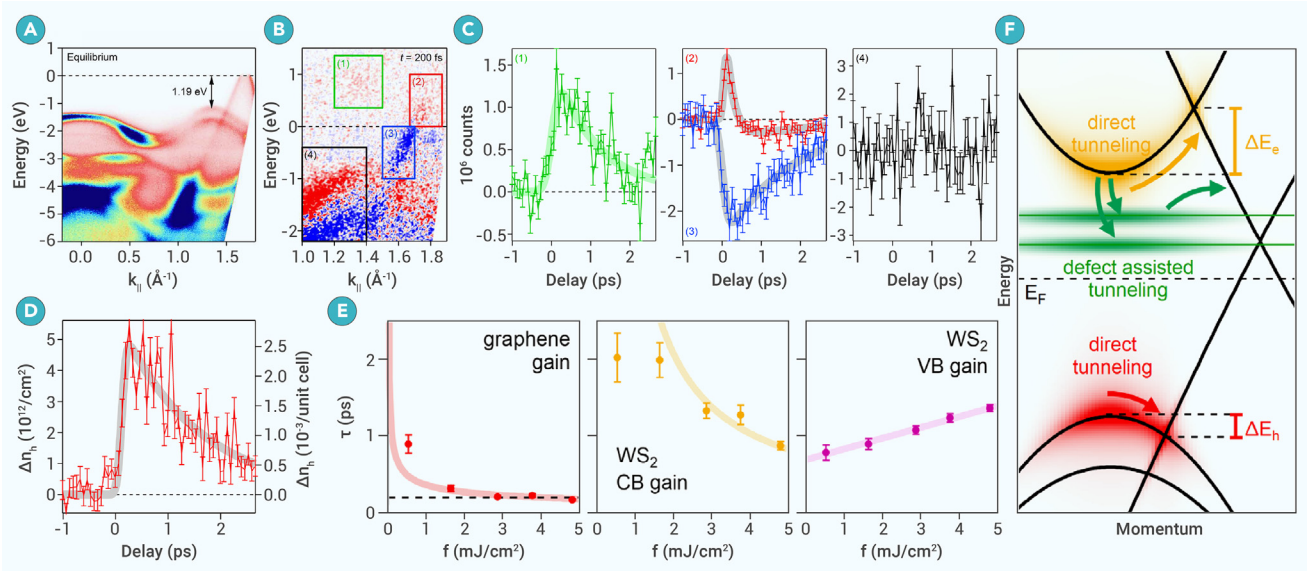

Figure 3. Experimental evidence of CT (A and B) Equilibrium photocurrent (A) and pump-induced photocurrent (B) change in a graphene-WS_2 vdWH. (C) Transient carrier population dynamics in the WS_2 conduction band (green), π-band of graphene above (red) and below (blue) the equilibrium chemical potential, and WS_2 valence band (black). (D) Transient hole density in the graphene layer. (E) Pump-fluence dependence of CT and charge separation time. (F) Possible CT channels. (A–D) Reproduced with permission.[68] Copyright 2020, AAAS. (E and F) Reproduced with permission.[83] Copyright 2021, American Physical Society.

intensity of the G and 2D modes. In contrast, ET only induces T_e changes, characterized by a transient decrease in 2D-mode intensity and G-mode broadening.[107] As shown in Figures 4A–4C, no significant transient intensity changes were observed in the G mode after photoexcitation. However, the 2D-mode intensities in both graphene and graphene-WS_2 vdWHs exhibit a transient decrease associated with increasing T_e, albeit at different decay rates. As shown in Figure 4D, T_e in bare graphene exhibits a fast decay (0.6 ps) due to ultrafast energy release into the phonon bath and substrate; T_e in WS_2-encapsulated graphene undergoes a slower decay (4.3 ps), which is attributed to the Förster-type ET from WS_2 to graphene (Figure 4E).[108]

Froehlicher et al.[74] examined CT/ET in graphene-$MoSe_2$ vdWHs by combining micro-photoluminescence (PL) and Raman scattering spectroscopies. This combination allowed for the exploration of CT/ET-induced perturbations on intrinsic radiative recombination in $MoSe_2$ and electron-phonon relaxation in graphene. As shown in Figures 5A and 5B, the PL intensity in the coupled graphene-$MoSe_2$ region is quenched by more than two orders of magnitude compared to the bare $MoSe_2$ region and increases linearly with the incident photon flux (ϕ_{ph}). Based on these observations, the authors proposed that interlayer coupling created a non-radiative pathway that significantly shortened the exciton lifetime in $MoSe_2$. Comprehensive analysis of ϕ_{ph}-dependent Raman-active modes and PL quenching efficiency (Figures 5C and 5D) revealed a critical transition (at ~290 ± 15 meV above the Dirac point in graphene) from photo-induced CT to ET.[82]

Another key factor affecting CT-ET competition is photon energy. For example, a tr-ARPES study by Dong et al.[79] reported CT-ET crossover in graphene-WSe_2 vdWHs by tuning the photon energy. They found that selective excitation of

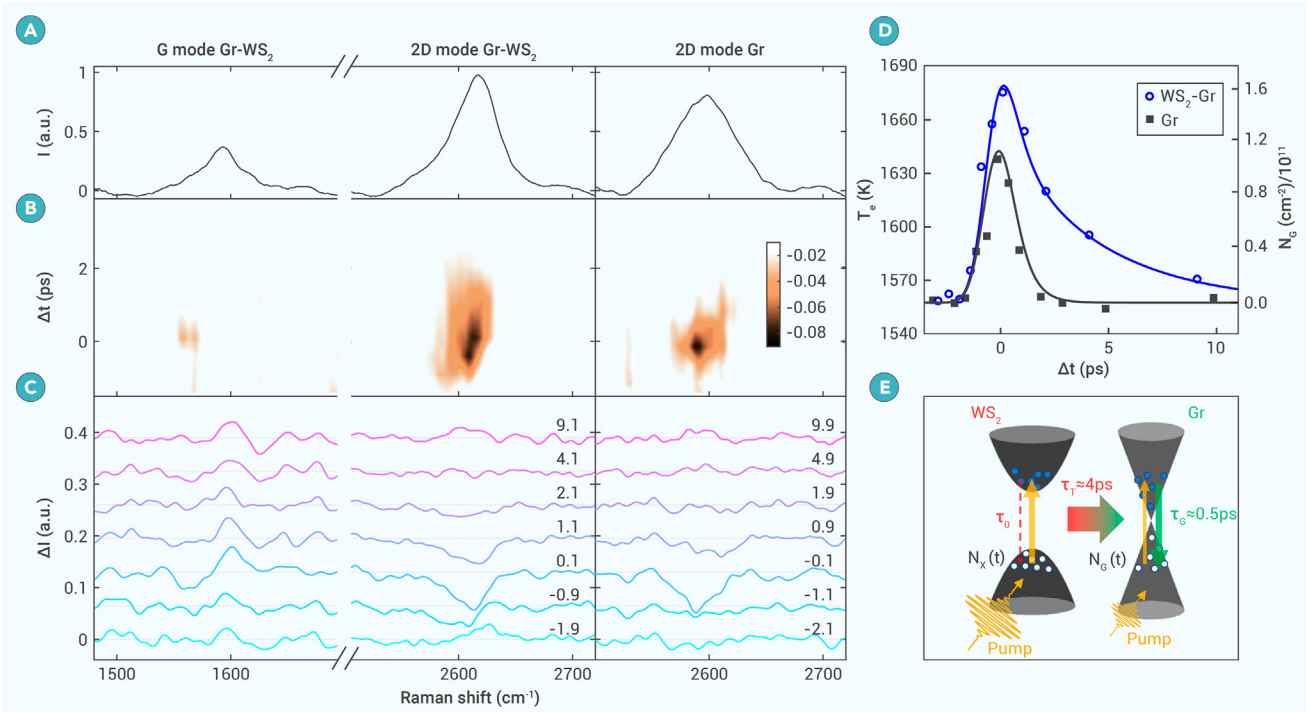

Figure 4. Experimental evidence of ET (A) Pump-off Raman spectra of a graphene-WS_2 vdWH. (B and C) Transient differential Raman spectra. (D) Time-dependent electronic temperature and carrier density. (E) Schematic of ET. (A–E) Reproduced with permission.[101] Copyright 2022, National Academy of Sciences, USA.

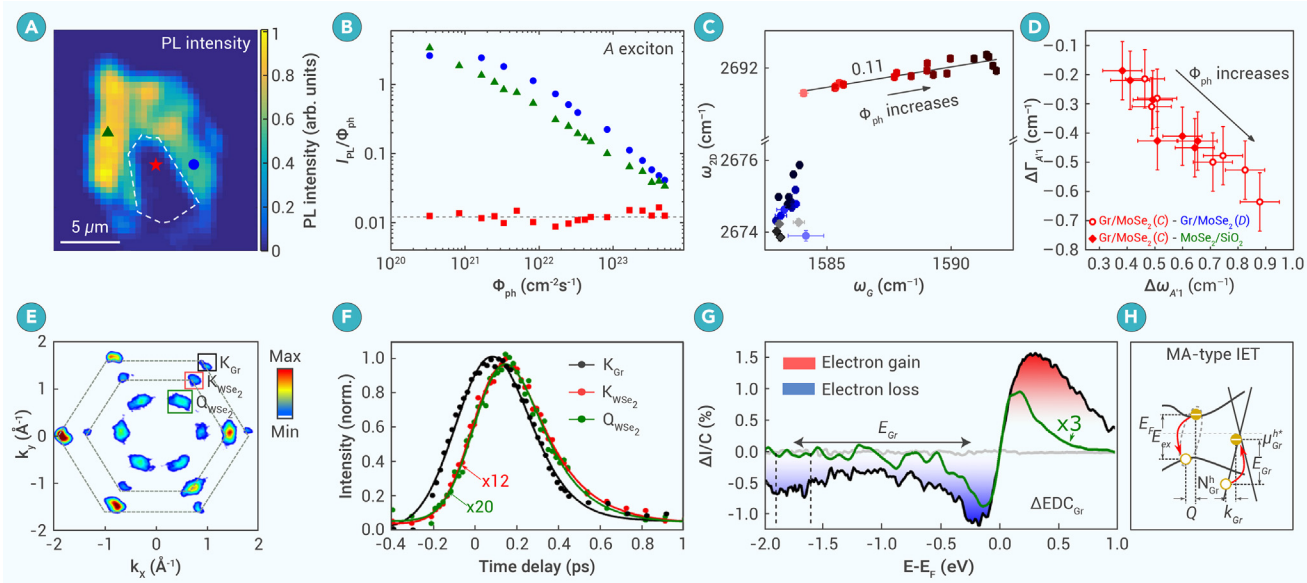

Figure 5. Competition between CT and ET (A) Photoluminescence mapping in a graphene-$MoSe_2$ vdWH. Dashed line indicates the contours of the graphene layer. (B) Photon-flux-normalized PL intensity versus incident photon flux from locations indicated in (A). (C and D) Raman signal analysis with increasing incident photon flux. (E) Momentum map of different excited states. (F) Normalized valley-dependent population dynamics. (G) Normalized momentum-integrated spectrum of graphene. (H) Schematic of Meitner-Auger ET. (A–D) Reproduced with permission.[74] Copyright 2018, American Physical Society. (E–H) Reproduced with permission.[79] Copyright 2023, Springer Nature.

graphene by below-band-gap photoexcitation populated the *K* and *Q* valleys in the WSe_2 conduction band (Figure 5E), which was delayed with respect to the rise of the hot-carrier population in graphene by ~50 fs (Figure 5F). Hot electrons with sufficiently high excess energy were proposed to overcome the interfacial energy barrier to occupy different valleys in WSe_2 through phonon-assisted interlayer tunneling and intervalley scattering. In contrast, following near-resonant photoexcitation, deep-lying valence hole populations with an energy difference of ~1.6 eV compared to E_F were measured in graphene (Figure 5G). The observed energy difference matched precisely the A-exciton resonance in WSe_2. Together with the rapid depletion dynamics of the exciton population in WSe_2, they interpreted this effect by the Meitner-Auger ET scenario: the annihilation of excitons in WSe_2 drives the intraband excitation of deep-lying valence electrons in graphene into empty hole states below the Dirac point (Figure 5H). This intraband excitation excludes the interband Förster-type ET mechanism, which is supported by simulations.

These findings suggest that the branching ratio between CT and ET can be tuned by controlling photoexcitation conditions, facilitating advanced optoelectronic devices with sophisticated functionalities. On the other hand, different tools have different sensitivities to CT and ET and operate in different excitation density regimes; for instance, extremely strong photoexcitation conditions were usually employed in tr-ARPES studies. A unified picture of the competition between CT and ET, in the same sample with complementary tools under widely tunable photoexcitation conditions, is still missing and requires further investigation.

CT AND RECOMBINATION MECHANISMS

The successful demonstration of CT and ET and the ability to modulate their competition has inspired further understanding of transfer and recombination mechanisms. In the following, we summarize recent spectroscopic efforts that have shed light on the intriguing phenomena associated with interfacial CT and recombination in graphene-semiconductor vdWHs. We will particularly focus our discussions on hot-carrier injection, defect-involved interfacial charge separation, and the buildup of interfacial electric fields following CT. These three highlighted topics are not only of fundamental research interest but also have far-reaching implications for relevant applications: (1) interfacing graphene with energy-selective contacts allows for the extraction of hot carriers from graphene,[109–111] relevant for efficient detection of sub-band-gap photons with high photoresponsivity and broad spectral sensitivity.[112,113] (2) Recent studies have revealed the potential of defects to prolong interfacial charge separation times through charge trapping.[23,75] This mechanism enables one type of carrier to recirculate in graphene while the other type remains trapped in defect states. The effect has been demonstrated to result in high photoconductive gain in photodetectors through the photogating effect.[9,24,95] (3) Elucidating the direction of the interfacial gating field can provide insights into the propagation direction of the generated photocurrent, thereby offering fundamental guidance for device operation and advanced controls.[77]

Thermalized versus non-thermalized: Hot-carrier dissociation at atomically thin interfaces

Along with donating charge/energy from the semiconductor to graphene, another attractive topic in graphene-semiconductor vdWHs is harvesting hot carriers from graphene before they dissipate their excess kinetic energy in the form of lattice heat: a concept at the heart of hot-carrier optoelectronics.[17,114–117] Fundamentally, exciting graphene with a photon energy greater than twice the E_F produces nascent, non-thermalized high-energy carriers (Figure 6A). Subsequently, a rapid thermalization process sets in within tens of fs due to efficient carrier-carrier scattering in graphene,[19,119,120] producing thermalized hot carriers that follow a Fermi-Dirac distribution with elevated electron temperature (Figure 6B). While photocurrents arising from hot carriers have been demonstrated in device studies,[17,121] a long-standing controversy has been whether carrier injection occurs before or after thermalization.

Chen et al.[118] investigated photoexcited carrier injection from graphene into WS_2 using ultrafast transient reflectance (TR) spectroscopy. In their study, graphene was selectively excited by below-band-gap photoexcitations, and the excited-state population in WS_2 was probed by the pulsed white-light continuum. Following hot-carrier injection from graphene into WS_2, broadening and band-filling effects of the A-exciton resonance in WS_2 were observed. The corresponding TR kinetics (Figure 6C) showed a rise time of 27 ± 4 fs and a decay time of ~1.2 ps, which were attributed to hot-electron transfer from graphene to WS_2 and the subsequent back-transfer process, respectively. By measuring fluence-dependent TR kinetics under different photon energies (Figure 6D), a hot-carrier injection quantum yield of up to 50% was claimed. More importantly, the yield was found to only depend on the photon energy rather than the pump fluence. In their scenario, the non-thermalized high-energy electrons and holes evolved into independent quasi-thermalized hot-carrier distributions with their own T_e and chemical potentials through intraband scattering, and hot-carrier injection occurred within tens of fs prior to electron-hole interband coalescence and thermalization.[122]

Recently, hot-carrier injection in the same heterostructure was investigated by optical-pump THz-probe (OPTP) spectroscopy.[23] In OPTP measurements, an ultrashort fs laser with tunable photon energy selectively excites the graphene layer or the heterostructure, and a time-delayed THz pulse characterizes the photoconductivity. The graphene layer dominates the photoconductivity due to its large charge mobility.[123] As shown in Figure 6E, below-band-gap photoexcitation

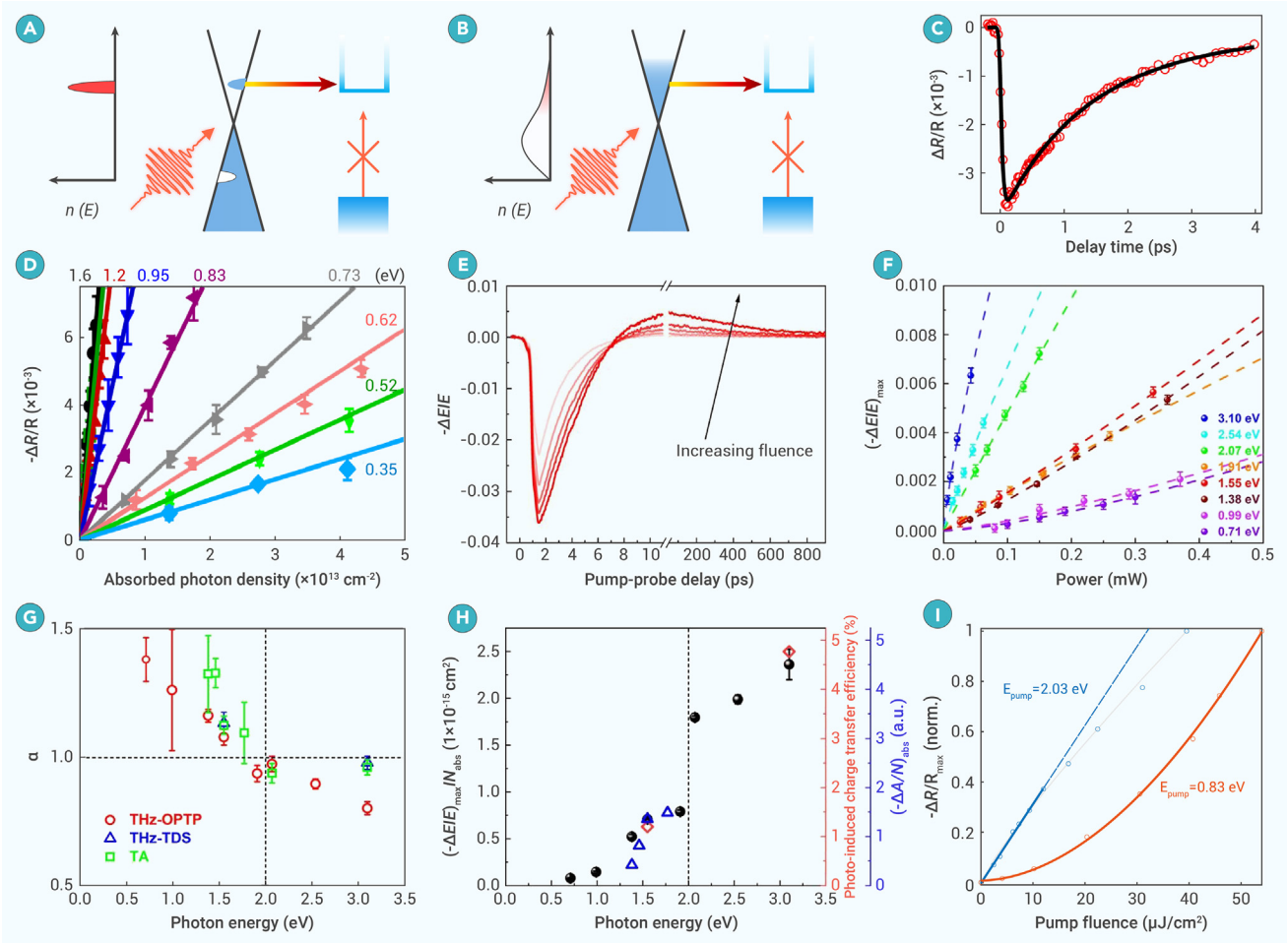

Figure 6. Hot-carrier transfer in a graphene-WS_2 vdWH (A and B) Schematics showing hot-electron transfer from graphene (A) before and (B) after thermalization. (C) TR trace at WS_2 A-exciton bleaching following 1.6 eV photoexcitation. (D) Fluence-dependent TR intensity at different photon energies. (E) Fluence-dependent CT dynamics following 1.38 eV photoexcitation. (F) Fluence-dependent photoconductivity at different photon energies. (G) Photon-energy-dependent power index obtained by different methods. (H) Quantification of photon-energy-dependent CT efficiency. (I) Normalized fluence-dependent TR intensity at different photon energies. (C and D) Reproduced with permission.[118] Copyright 2019, AAAS. (E–H) Reproduced with permission.[23] Copyright 2021, AAAS. (I) Reproduced with permission.[69] Copyright 2022, Springer Nature.

yields a transient reduction in conductivity, i.e., a negative photoconductivity. The effect has been widely reported in graphene away from the Dirac point and is associated with hot carriers having lower mobility than cold ones.[19,124–127] Strikingly, the transient photoconductivity was found to undergo a sign change within 10 ps after photoexcitation, showing a long-lived positive photoconductivity. This was attributed to the downward shift of E_F of the initially p-doped graphene following hot-electron injection into WS_2. By relating the fluence-dependent positive photoconductivity to the photon energy, an intriguing transition in the CT mechanism was noticed (Figures 6F–6H): for below-band-gap excitations, the CT-induced photoconductivity exhibited a superlinear relationship with the pump fluence, indicating that thermalized hot electrons with sufficiently high energy could be injected to WS_2 via photo-thermionic emission with relatively low efficiency (~1%). For above-band-gap excitations, the CT-induced photoconductivity was shown to scale linearly with the pump fluence. This effect was attributed to direct hole transfer from the WS_2 valence band to graphene with a relatively high efficiency (~5%). A subsequent TR study[69] reproduced the revealed dependence of photon energy on the exciton photobleaching signal (Figure 6I). Benefiting from the high temporal resolution, the sub-20 fs rise observed in the TR kinetics sets the ultimate timescale for thermalized hot-electron transfer. Furthermore, an alternative scenario for the observed exciton photobleaching signal following below-band-gap excitations involved the direct excitation of interlayer CT transitions. As proposed by Yuan et al.,[70] this scenario relies on momentum-allowed direct transitions, thereby requiring a minimum photon energy of ~1 eV. Although theoretically possible, this scenario alone failed to explain the CT phenomena observed at sub-1 eV photon excitations.[118]

Overall, despite the demonstration of hot-carrier injection, whether it occurs before or after thermalization remains controversial. One possible origin of this controversy is sample differences in interfacial coupling strength, homogeneity, doping, and twist angle, all of which may contribute to the competition between thermalization and hot-carrier injection. Further studies incorporating ultimate spatial, temporal, and spectral resolution and control variables may clarify this controversy.

The role of defects in interfacial charge separation lifetime

Following CT, charge carriers with opposite signs reside in different layers, forming a transient charge-separated state whose lifetime is critical for photocatalysis and photodetectors.[24,128–130]

Jnawali et al.[78] used OPTP spectroscopy to examine interfacial dynamics in graphene-C_{60} vdWHs. They showed that graphene-C_{60} vdWHs exhibited positive photoconductivity with a lifetime of ~100 ps (Figure 7A), associated with photo-induced hole transfer from C_{60} to the initially p-doped graphene. The long-lived nature of interfacial charge separation was rationalized by the presence of in-gap defect states, which rapidly trap the remaining electrons in C_{60} following photo-induced hole transfer from C_{60} to graphene (Figure 7B), in C_{60} due to its exposure to oxygen.[131,132] The localized nature of the defect state reduces the interfacial recombination probability, prolonging the interfacial charge separation lifetime.

Our recent study[23,111] also elucidated the role of defects in interfacial charge separation in graphene-WS_2 vdWHs by complementarily measuring the ultrafast photoconductivity in graphene (Figure 7C) and the excited-state dynamics in WS_2 (Figure 7D). While transient absorption (TA) reported a short excited-state lifetime (~1 ps; Figure 7E) in WS_2, OPTP showed long-lived photoconductivity (over 1 ns; Figure 7F). The discrepancy between the carrier lifetimes in the electron donor (graphene) and acceptor (WS_2) can be rationalized by the presence of

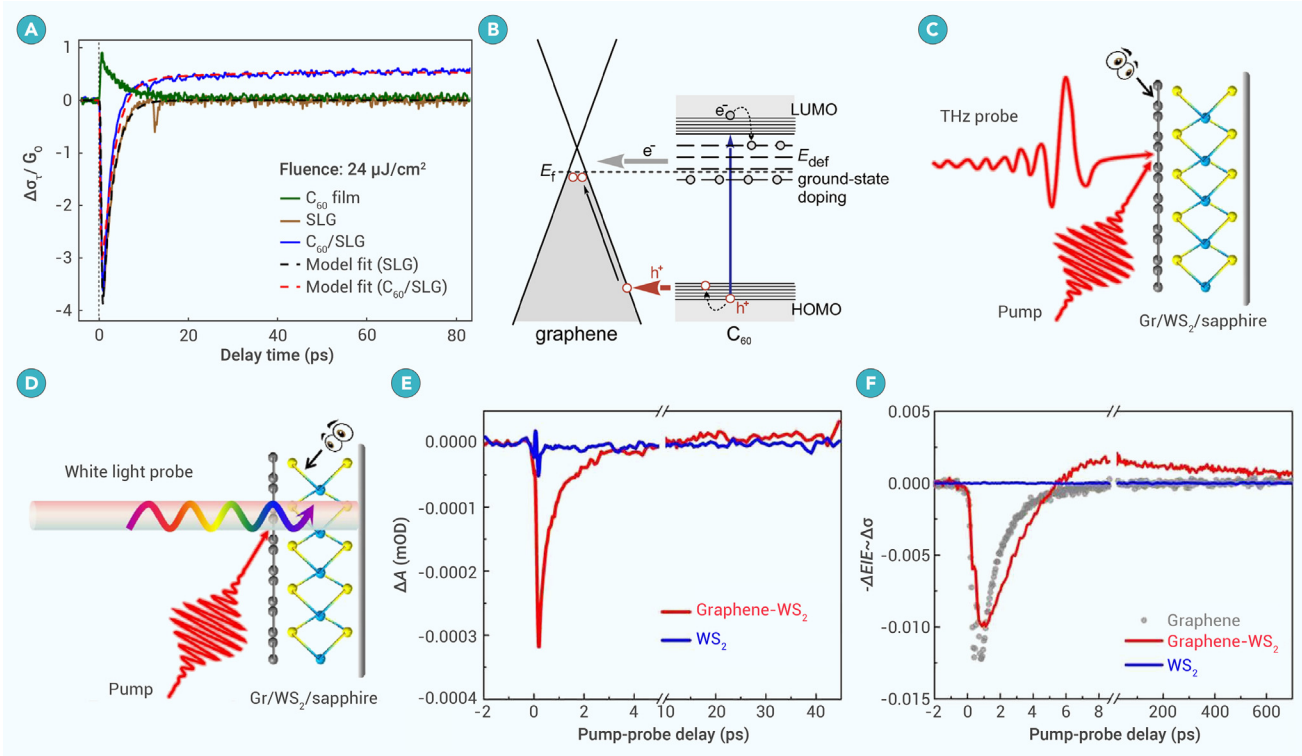

Figure 7. Defect-induced long-lived interfacial charge separation (A) Photoconductivity dynamics following 3.1 eV photoexcitation of C_{60}, graphene, and their heterostructure. (B) Schematic showing photo-induced hole transfer from C_{60} to single-layer graphene (SLG) and trapping of photogenerated electrons at defects. (C and D) Schematics showing the schemes and sensitivities of complementary (C) OPTP and (D) TA measurements. (E) TA traces of the A-exciton photobleaching following 1.55 eV photoexcitation. (F) Photoconductivity dynamics following 1.55 eV photoexcitation. (A and B) Reproduced with permission.[78] Copyright 2015, American Chemical Society. (C–F) Reproduced with permission.[23] Copyright 2021, AAAS.

defect states. These defect states can capture injected electrons in WS_2 within 1 ps and store them further for ~1 ns before recombining with photogenerated holes in graphene. This leads to a long-lived photogating effect in graphene, contributing to the ultrahigh photoconductive gain in high-performance photodetectors.[96–98] Recent scanning tunneling microscopy studies and *ab initio* theoretical calculations indicated that sulfur vacancies in WS_2 could generate two unoccupied in-gap electronic states,[133,134] which are very likely the origin of the defect states leading to the observed long-lived interfacial charge separation.

Overall, these results revealed the bright side of defects: although they are generally considered detrimental to electronic devices, they can benefit optoelectronic applications by extending the charge separation time and inducing photogating effects once properly controlled. This promising prospect inspires the microscopic understanding of defect origins and the management of defect types and densities through defect engineering.

Understanding the interfacial electric field direction

An important consequence of CT is the generation of an interfacial electric field directed between components. Understanding the direction of the interfacial electric field not only has fundamental research implications but also paves the way for designing novel optoelectronic functionalities.

Following CT, interfacial electric fields with opposite directions (i.e., directed from/to graphene) were recently reported in different graphene-based vdWHs.[26,135] Employing helicity-resolved TA spectroscopy, Zhou et al.[66] found that the band offset for electron/hole transfer ($\Delta E_e/\Delta E_h$) played an important role in determining the interfacial electric field direction, due to the linear relationship between $\Delta E_e/\Delta E_h$ and the density of states available for accepting electrons/holes in graphene. For graphene-WS_2 vdWHs, where $\Delta E_h > \Delta E_e$, photo-induced hole transfer from WS_2 to graphene was found to be much faster than electron transfer (210 fs versus 1.43 ps), resulting in a transient interfacial electric field directed from graphene to WS_2 (Figures 8A and 8B). In contrast, for graphene-WSe_2 vdWHs, where $\Delta E_e > \Delta E_h$, photogenerated electrons showed a higher CT rate from WSe_2 to graphene than holes (150 fs versus 2.28 ps), leading to a transient interfacial electric field directed from WSe_2 to graphene (Figures 8C and 8D).

Furthermore, Zhang et al.[77] demonstrated an optical switching of the interfacial charge flow direction in graphene-$Cs_2AgBiBr_6$ vdWHs by adjusting the photon energy. As shown in Figures 8E–8H, above-band-gap photoexcitation yielded CT-induced positive photoconductivity that scaled sub-linearly with the pump fluence, which could be attributed to the transfer of photogenerated holes from $Cs_2AgBiBr_6$ to graphene. Below-band-gap photoexcitation led to CT-induced negative photoconductivity that was linearly dependent on the pump fluence, suggesting that the dominant CT mechanism was related to the direct transfer of high-energy holes from graphene to the in-gap defect states in $Cs_2AgBiBr_6$. The revealed photon-energy-dependent CT mechanism allowed modulation of the interfacial charge flow direction, providing an all-optical way to tune photogating fields that are highly relevant for photodetection.

CONTROLLING ULTRAFAST CHARGE FLOW ACROSS GRAPHENE-SEMICONDUCTOR vdW INTERFACES

Tracking and understanding the mechanisms, directions, and pathways of charge/energy flow inspires further exploration of their determining parameters, aiming to guide the design and operation of advanced optoelectronic devices. Below, we summarize recent spectroscopic efforts to explore the control knobs that modulate charge/energy flow in graphene-semiconductor vdWHs, including vdW interactions and defect modulation.

Tuning vdW interactions

The interfacial coupling strength governed by vdW interactions plays a key role in determining CT efficiency. Thanks to the strong interfacial π-π interactions, the hybridization of graphene and its nanoscale segment nanographene (NG) is considered a promising strategy to construct vdWHs with tunable vdW interactions and band alignment. As shown in Figure 9A, Gobre et al.[136] showed that vdW interactions in various carbon-based systems are characterized by peculiar scaling laws, depending on the dimensionality and size of the system. Inspired by this, Yu et al.[76] investigated NG-size-dependent CT dynamics in graphene-NG interfaces using OPTP spectroscopy. By increasing the size of NG, the interfacial coupling strength between NG and graphene is expected to greatly increase, even though the interfacial energy difference driving the CT process is unfavorably reduced (Figure 9B). As shown in Figures 9C–9E, remarkably, the CT efficiency was shown to increase by an order of magnitude when the size of NG in the polyaromatic core is increased from 42 to 96 carbon atoms, thanks to

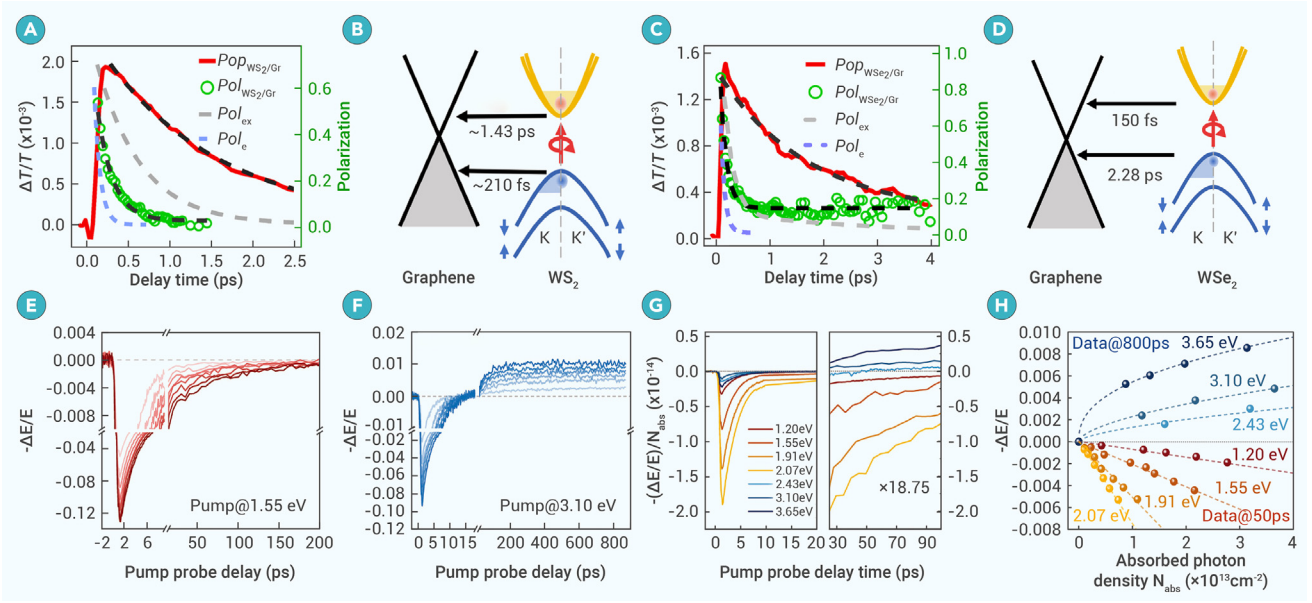

Figure 8. Interfacial charge flow direction (A and B) Population and polarization kinetics of a graphene-WS_2 vdWH following 2.05 eV photoexcitation (A) and corresponding asynchronous CT schematic (B). (C and D) Population and polarization kinetics of graphene-WSe_2 vdWHs following 1.72 eV photoexcitation (C) and corresponding asynchronous CT schematic (D). (E and F) Fluence-dependent photoconductivity dynamics following (E) 1.55 eV and (F) 3.10 photoexcitation. (G and H) Photon-energy-dependent photoconductivity dynamics and intensity comparison. (A–D) Reproduced with permission.[66] Copyright 2021, AAAS. (E–H) Reproduced with permission. Copyright 2023, Wiley.[77]

the greatly enhanced interfacial coupling strength. These findings provided insights into designing all-carbon-based vdWHs containing graphene and large-sized NGs for efficient, low-toxicity photodetection.[26]

Defect control

As discussed, recent studies revealed that defects play a key role in determining the charge separation lifetime in graphene-semiconductor vdWHs.[23,111] In particular, sulfur vacancies have been reported to introduce two in-gap defect states with a typical density of 10^9–10^{13} cm^{-2}.[137,138] As such, modulating defect occupancy is expected to be an effective strategy to control interfacial charge flow. For that, a recent study[75] investigated interfacial CT dynamics in graphene-WS_2 vdWHs while tuning the charge filling of defect states by *operando* OPTP measurements (Figure 10A). Figure 10B exhibits the photoconductivity dynamics operating at different gate voltages following below-gap photoexcitation. The CT-induced photoconductivity and resulting local photogating field demonstrated non-trivial dependence on gate voltage (Figure 10C). Notably, the local

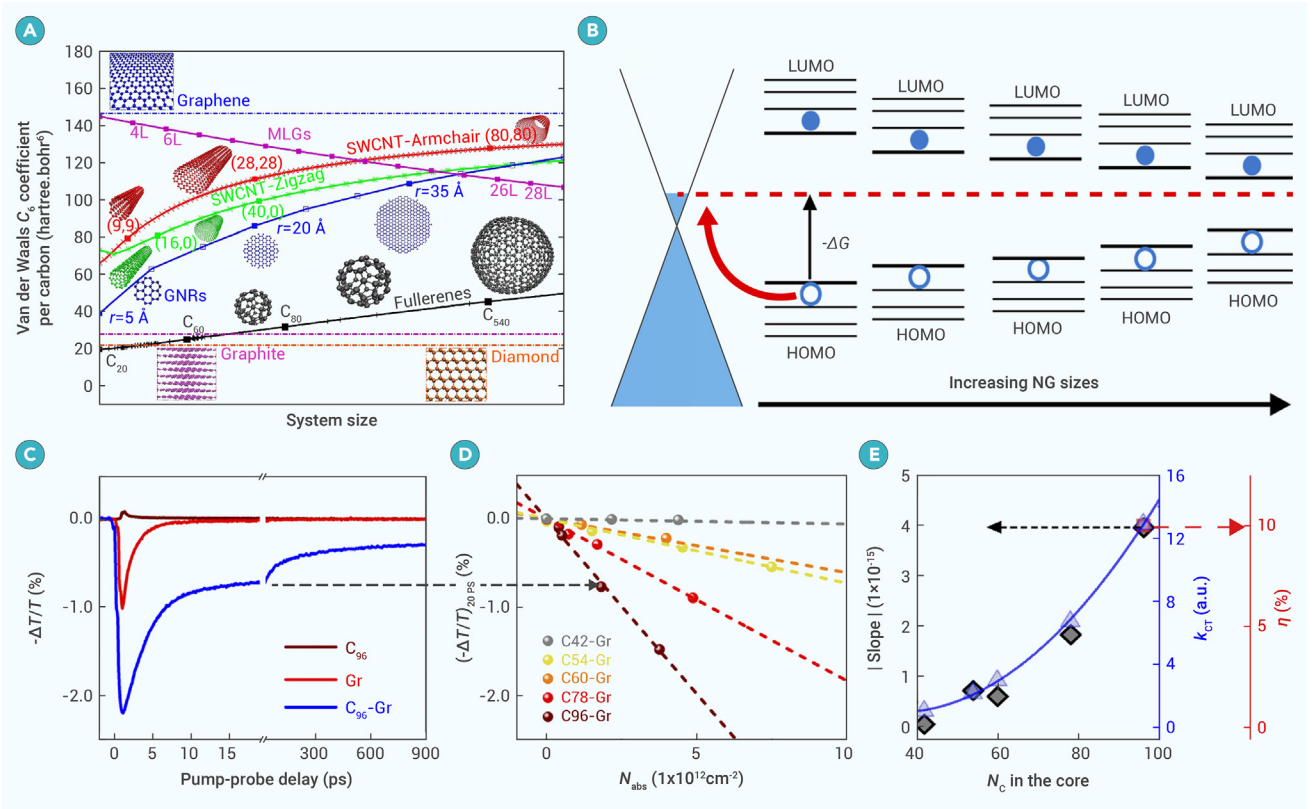

Figure 9. Tuning the CT efficiency by engineering vdW interactions (A) Scaling laws for vdW coefficients. (B) Schematic of the band alignment and photo-induced CT. (C) Photoconductivity dynamics following 3.1 eV photoexcitation. (D) Photoconductivity for different graphene-NG vdWHs versus absorbed photon density. (E) Size-dependent photo-induced hole transfer efficiency. (A) Reproduced with permission.[136] Copyright 2013, Springer Nature. (B–E) Reproduced with permission. Copyright 2022, AIP Publishing.[76]

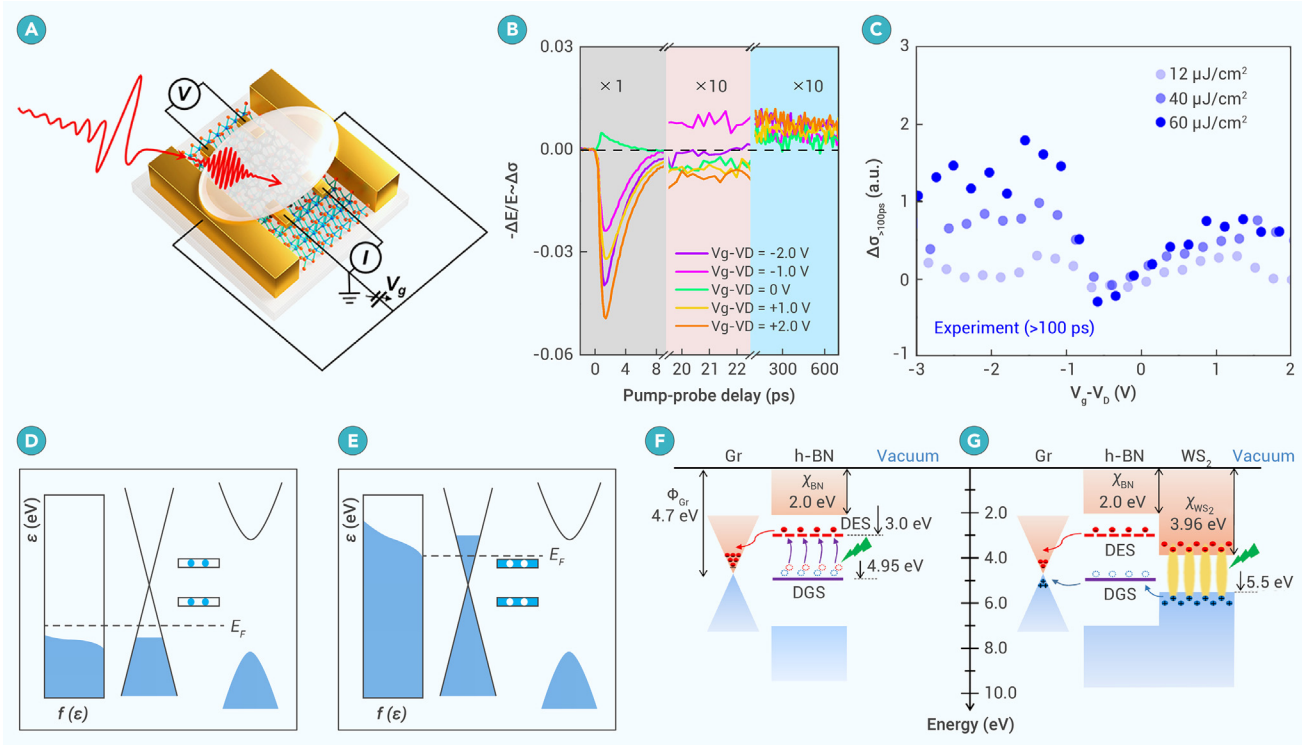

Figure 10. Tuning charge and energy flow by intrinsic and extrinsic defects (A) Schematic of *operando* OPTP measurements. (B) Photoconductivity dynamics at the graphene-WS_2 vdW interface operated at different gate voltages. (C) Fluence-dependent photoconductivity averaged from 100 to 700 ps versus gate voltage. (D and E) Snapshots illustrating the photogating mechanisms in (D) p-doped and (E) n-doped graphene-WS_2 vdWHs. (F and G) Schematics showing the interfacial relaxation pathways without (F) and with (G) the WS_2 top layer. (A–E) Reproduced with permission.[75] Copyright 2023, ACS Chemical Society. (F and G) Reproduced with permission.[71] Copyright 2020, ACS Chemical Society.

photogating field was found to switch from electron photogating (e.g., with long-lived positive photoconductivity) when the defect states were empty to hole photogating (e.g., with long-lived negative photoconductivity) when the defect states were filled. The observed electrically tunable photogating dynamics were well reproduced by simulating CT via photo-thermionic emission and involving two in-gap defects as donors or acceptors for CT (depending on occupancy): in p-doped heterostructures with unoccupied defect states, photo-induced electron injection or trapping into defects in WS_2 governed the photogating mechanism, leading to an electron photogating effect (Figure 10D); in n-doped heterostructures with occupied defect states, photogenerated holes were injected into defects, resulting in a hole photogating scheme (Figure 10E).

Apart from exploiting the intrinsic defect states originating from building blocks, the introduction of extrinsic defect states has also been shown to affect interfacial relaxation pathways. For example, Liu et al.[71] manipulated the nature of the charge flow injected into graphene by jointly exploiting defect states in *h*-BN spacers and the stacking tunability of graphene-*h*-BN-WS_2 vdWHs. They found that, in the absence of the WS_2 top layer, photoexcitation triggers the ground-to-excited-state transition of defect states in *h*-BN and results in a net electron injection into graphene, raising E_F in graphene up to ~120 meV (Figure 10F), while in the presence of the WS_2 top layer, photo-induced hole relaxation from WS_2 to *h*-BN to graphene is enabled (Figure 10G). Such cascaded hole transfer neutralizes the electron injection from *h*-BN defect states to graphene, making graphene an energy acceptor with negligible net charge accumulation.

PERSPECTIVES

Defect engineering

Although the critical role of defects in determining charge separation and the photogating mechanism has been well demonstrated,[23,71,75] the precise characterization and control of defect type and density remain challenging since they are often sample specific and strongly influenced by synthesis history. Further engineering of the defect type (e.g., by O^{2+} plasma treatment[139]) and density (e.g., by electron beam irradiation[140] or chemical healing[141]) is necessary to activate the full potential of defects in optimizing application performance. Furthermore, controlling defect occupancy or chemical potential using electrostatic or electrochemical gating[142,143] provides an alternative control knob for the strength and direction of the interfacial electric field.

Organic-inorganic 2D vdW interfaces

Compared to the widely explored graphene-inorganic vdWHs, the field of graphene-organic vdWHs remains less studied, despite its potential. In particular, the infinite tunability of chemical structures and the solution processability of organic materials make graphene-organic vdWHs promising for large-scale and low-cost device integration.[144] One major challenge hindering the development of graphene-organic vdWHs lies in the difficulty of achieving homogeneous and compact deposition/growth of long-range-ordered organic structures on graphene, which is essential for forming strongly coupled heterostructures. Recent progress in synthesizing high-quality crystalline organic structures, such as covalent organic frameworks (COFs) and metal-organic frameworks (MOFs), offers promising avenues for overcoming this barrier.[145] For instance, Han et al.[146] recently demonstrated a $CF_3COOH/CF_3CH_2NH_2$ protocol that enabled the rapid growth of single-crystal COFs with crystal sizes of up to 150 μm. Wang et al.[147] synthesized monolayer Cu_3BHT with μm^2-scale uniformity and atomic flatness using on-water surface chemistry. The assembled graphene-Cu_3BHT vdWHs exhibited efficient photo-induced interlayer charge separation, achieving a net electron transfer efficiency of up to 34% from Cu_3BHT to graphene. Liu et al.[148] developed an on-liquid-gallium surface synthesis strategy under chemical vapor deposition (CVD) conditions, where the high adhesion energy between gallium and planar aromatic ligands promoted the layer-by-layer growth of ultra-smooth MOF films with a surface roughness as low as ~2 Å. These rapid advances in controlling the crystal size, layer number, and surface roughness of 2D crystalline organic structures, combined with the vast molecular design space, pave the way for engineering interface energetics, tuning interfacial charge and energy flow, and device integration. Future efforts should prioritize the development of new graphene-organic vdWHs and establish universal methods for fabricating high-quality graphene-organic vdWHs. These advances will make it possible to explore new interfacial phenomena that are inaccessible with inorganic counterparts.

Graphene-Janus TMDC heterostructures

In 2017, Lu et al.[149] synthesized the first Janus TMDC, MoSSe, using a two-step CVD process. In the synthesis, the authors used remote H_2 plasma to strip off the top-layer S atoms in MoS_2, followed by thermal selenization to replace H atoms with Se atoms. The resulting symmetry breaking in the out-of-plane direction induces an intrinsic vertical piezoelectric response and a large Rashba

spin-orbit interaction, which are relevant for nanoelectromechanical devices and spintronics, respectively. On this basis, Liu et al.[150] proposed that the intrinsic built-in electric field within the monolayer Janus TMDC, originating from the difference in electronegativity between S and Se, leads to an asymmetry potential when sandwiched by two graphene layers. This asymmetry potential enables the efficient and spontaneous separation of photogenerated electrons and holes into different graphene layers on the timescale of hundreds of fs upon light absorption. Using first-principles density functional theory (DFT) calculations and *ab initio* nonadiabatic molecular dynamics simulations, they demonstrated that photogenerated electrons (holes) can be transferred from monolayer MoSSe (MoSeTe) to the graphene layer on the Se side with a lower (higher) potential, while the transfer of the photogenerated holes (electrons) is inhibited due to the significant separation between the donor and acceptor states. These hypotheses call for future experimental work using ultrafast spectroscopies to verify these concepts and for device engineering to exploit the potential of Janus heterostructures for, e.g., light-sensing applications.

Spin injection

Graphene-based vdWHs also provide a new platform for exploring opto-spintronics.[151] Because of its high mobility, weak spin-orbit coupling (SOC), and minimal hyperfine interactions, graphene has been recognized as a promising material in spintronics, characterized by long spin lifetimes and relaxation lengths.[152,153] However, its application in opto-spintronics is limited by the absence of spin-dependent optical selection rules. One approach to overcome this limitation is to combine graphene with 2D semiconductors that possess strong SOC to form vdWHs. Growing evidence suggests that TMDCs with exceptional spin-valley coupling are promising candidates for spin injection into graphene when excited with circularly polarized light.[28,39] This not only mitigates the issue of contact conductance mismatch but also introduces new mechanisms to control spin injection.[66] Besides, the stacking orders and twisting of adjacent layers can provide further means to manipulate spin injection and spin transport. Another attractive vdW system for spin injection is intrinsic 2D magnets, such as semiconducting CrI_3 and metallic Fe_3GeTe_2.[154] The proximity-induced exchange effect between graphene and these 2D magnetic materials opens up rich possibilities for engineering novel functionalities in (opto-)spintronics. While light-induced spin transfer promises ultrafast control of data recording and processing with least-dissipative power consumption, further efforts are needed to explore these systems' ultrafast spin transfer dynamics to fully unveil their potential.

CONCLUSION

In conclusion, this review summarizes recent advances in understanding and controlling ultrafast CT/ET phenomena in graphene-semiconductor vdWHs and discusses their potential implications for optoelectronic applications. Various ultrafast spectroscopies, each with distinct sensitivities to CT and ET, provide different perspectives on how charge or energy flow traverses the graphene-semiconductor interface and how the interfacial separation state is reset over longer timescales. Growing evidence indicates that CT and ET are competing ultrafast interfacial relaxation channels occurring on timescales of tens to hundreds of fs, with their competition influenced by photoexcitation conditions (i.e., pump fluence and wavelength). By collecting recent studies, this review comes up with three intriguing topics that are particularly critical to device performance: the mechanism of hot-carrier injection, the beneficial role of defects in extending interfacial charge separation, and the direction of CT-induced interfacial electric fields. We hope these insights inspire further ultrafast spectroscopic studies to address existing controversies. Furthermore, we propose a rudimentary toolkit—encompassing vdW interactions and defect engineering—to modulate charge and energy flow in graphene-semiconductor vdWHs, providing foundational guidance for designing high-performance optoelectronic devices. Finally, we expect that forthcoming breakthroughs in this field will emerge from collaborative efforts of materials science, ultrafast spectroscopy, and device integration to design novel vdWHs and explore fascinating interfacial phenomena.

REFERENCES

1. Bolotin, K.I., Sikes, K., Jiang, Z., et al. (2008). Ultrahigh electron mobility in suspended graphene. Solid State Commun. ***146***: 351–355.
2. Novoselov, K.S., Geim, A.K., Morozov, S.V., et al. (2004). Electric field effect in atomically thin carbon films. Science ***306***: 666–669.
3. Banszerus, L., Schmitz, M., Engels, S., et al. (2015). Ultrahigh-mobility graphene devices from chemical vapor deposition on reusable copper. Sci. Adv. ***1***: e1500222. https://doi.org/10.1126/sciadv.1500222.
4. Banszerus, L., Sohier, T., Epping, A., et al. (2019). Extraordinary high room-temperature carrier mobility in graphene-WSe_2 heterostructures. Preprint at: arXiv. 1909.09523. https://doi.org/10.48550/arXiv.1909.09523
5. Choi, H., Borondics, F., Siegel, D.A., et al. (2009). Broadband electromagnetic response and ultrafast dynamics of few-layer epitaxial graphene. Appl. Phys. Lett. ***94***: 172102. https://doi.org/10.1063/1.3122348.
6. Winnerl, S., Orlita, M., Plochocka, P., et al. (2011). Carrier relaxation in epitaxial graphene photoexcited near the Dirac point. Phys. Rev. Lett. ***107***: 237401. https://doi.org/10.1103/PhysRevLett.107.237401.
7. Nair, R.R., Blake, P., Grigorenko, A.N., et al. (2008). Fine structure constant defines visual transparency of graphene. Science ***320***: 1308.
8. Mak, K.F., Sfeir, M.Y., Wu, Y., et al. (2008). Measurement of the optical conductivity of graphene. Phys. Rev. Lett. ***101***: 196405. https://doi.org/10.1103/PhysRevLett.101.196405.
9. Koppens, F.H.L., Mueller, T., Avouris, P., et al. (2014). Photodetectors based on graphene, other two-dimensional materials and hybrid systems. Nat. Nanotechnol. ***9***: 780–793.
10. Xia, F., Mueller, T., Golizadeh-Mojarad, R., et al. (2009). Photocurrent imaging and efficient photon detection in a graphene transistor. Nano Lett. ***9***: 1039–1044.
11. Xia, F., Mueller, T., Lin, Y.M., et al. (2009). Ultrafast graphene photodetector. Nat. Nanotechnol. ***4***: 839–843.
12. Mueller, T., Xia, F., and Avouris, P. (2010). Graphene photodetectors for high-speed optical communications. Nat. Photonics ***4***: 297–301.
13. Gan, X., Shiue, R.J., Gao, Y., et al. (2013). Chip-integrated ultrafast graphene photodetector with high responsivity. Nat. Photonics ***7***: 883–887.
14. Pospischil, A., Humer, M., Furchi, M.M., et al. (2013). CMOS-compatible graphene photodetector covering all optical communication bands. Nat. Photonics ***7***: 892–896.
15. Schuler, S., Muench, J.E., Ruocco, A., et al. (2021). High-responsivity graphene photodetectors integrated on silicon microring resonators. Nat. Commun. ***12***: 3733.
16. Muench, J.E., Ruocco, A., Giambra, M.A., et al. (2019). Waveguide-integrated, plasmonic enhanced graphene photodetectors. Nano Lett. ***19***: 7632–7644.
17. Massicotte, M., Soavi, G., Principi, A., et al. (2021). Hot carriers in graphene–fundamentals and applications. Nanoscale ***13***: 8376–8411.
18. Johannsen, J.C., Ulstrup, S., Cilento, F., et al. (2013). Direct view of hot carrier dynamics in graphene. Phys. Rev. Lett. ***111***: 027403. https://doi.org/10.1103/PhysRevLett.111.027403.
19. Tielrooij, K.J., Song, J.C.W., Jensen, S.A., et al. (2013). Photoexcitation cascade and multiple hot-carrier generation in graphene. Nat. Phys. ***9***: 248–252.
20. Pogna, E.A.A., Jia, X., Principi, A., et al. (2021). Hot-carrier cooling in high-quality graphene is intrinsically limited by optical phonons. ACS Nano ***15***: 11285–11295.
21. Gierz, I., Petersen, J.C., Mitrano, M., et al. (2013). Snapshots of non-equilibrium Dirac carrier distributions in graphene. Nat. Mater. ***12***: 1119–1124.
22. Mihnev, M.T., Kadi, F., Divin, C.J., et al. (2016). Microscopic origins of the terahertz carrier relaxation and cooling dynamics in graphene. Nat. Commun. ***7***: 11617. https://doi.org/10.1038/ncomms11617.
23. Fu, S., du Fossé, I., Jia, X., et al. (2021). Long-lived charge separation following pump-wavelength-dependent ultrafast charge transfer in graphene/WS_2 heterostructures. Sci. Adv. ***7***: eabd9061. https://doi.org/10.1126/sciadv.abd9061.
24. Konstantatos, G., Badioli, M., Gaudreau, L., et al. (2012). Hybrid graphene–quantum dot phototransistors with ultrahigh gain. Nat. Nanotechnol. ***7***: 363–368.
25. Miao, X., Tongay, S., Petterson, M.K., et al. (2012). High efficiency graphene solar cells by chemical doping. Nano Lett. ***12***: 2745–2750.
26. Liu, Z., Qiu, H., Fu, S., et al. (2021). Solution-processed graphene–nanographene van der Waals heterostructures for photodetectors with efficient and ultralong charge separation. J. Am. Chem. Soc. ***143***: 17109–17116.
27. Sorcar, S., Thompson, J., Hwang, Y., et al. (2018). High-rate solar-light photoconversion of CO_2 to fuel: Controllable transformation from C_1 to C_2 products. Energy Environ. Sci. ***11***: 3183–3193.
28. Avsar, A., Unuchek, D., Liu, J., et al. (2017). Optospintronics in graphene via proximity coupling. ACS Nano ***11***: 11678–11686.
29. Guo, X., Liu, R., Hu, D., et al. (2020). Efficient all-optical plasmonic modulators with atomically thin van der Waals heterostructures. Adv. Mater. ***32***: 1907105. https://doi.org/10.1002/adma.201907105.
30. Mukherjee, B., Zulkefli, A., Watanabe, K., et al. (2020). Laser-assisted multilevel non-volatile memory device based on 2D van-der-Waals few-layer-ReS_2/h-BN/graphene heterostructures. Adv. Funct. Mater. ***30***: 2001688. https://doi.org/10.1002/adfm.202001688.
31. Wang, X., Cheng, Z., Xu, K., et al. (2013). High-responsivity graphene/silicon-heterostructure waveguide photodetectors. Nat. Photonics ***7***: 888–891.
32. Qiao, H., Yuan, J., Xu, Z., et al. (2015). Broadband photodetectors based on graphene–Bi_2Te_3 heterostructure. ACS Nano ***9***: 1886–1894.
33. Wu, J., Lu, Y., Feng, S., et al. (2018). The interaction between quantum dots and graphene: the applications in graphene-based solar cells and photodetectors. Adv. Funct. Mater. ***28***: 1804712. https://doi.org/10.1002/adfm.201804712.
34. Zhang, Z., Lin, P., Liao, Q., et al. (2019). Graphene-based mixed-dimensional van der Waals heterostructures for advanced optoelectronics. Adv. Mater. ***31***: 1806411. https://doi.org/10.1002/adma.201806411.

35. Singh, E., and Nalwa, H.S. (2015). Graphene-based bulk-heterojunction solar cells: a review. J. Nanosci. Nanotechnol. ***15***: 6237–6278.
36. Singh, E., and Nalwa, H.S. (2015). Stability of graphene-based heterojunction solar cells. RSC Adv. ***5***: 73575–73600.
37. Li, C., Cao, Q., Wang, F., et al. (2018). Engineering graphene and TMDs based van der Waals heterostructures for photovoltaic and photoelectrochemical solar energy conversion. Chem. Soc. Rev. ***47***: 4981–5037.
38. Behura, S.K., Wang, C., Wen, Y., et al. (2019). Graphene–semiconductor heterojunction sheds light on emerging photovoltaics. Nat. Photonics ***13***: 312–318.
39. Luo, Y.K., Xu, J., Zhu, T., et al. (2017). Opto-valleytronic spin injection in monolayer MoS_2/few-layer graphene hybrid spin valves. Nano Lett. ***17***: 3877–3883.
40. Li, X., Shen, R., Ma, S., et al. (2018). Graphene-based heterojunction photocatalysts. Appl. Surf. Sci. ***430***: 53–107.
41. Sajna, M.S., Simon, S.M., Unnikrishnan, N.V., et al. (2022). An overview of graphene-based 2D/3D nanostructures for photocatalytic applications. Top. Catal. 1–25. https://doi.org/10.1007/s11244-021-01539-5.
42. Li, Y., Zhang, D., Jia, R., et al. (2020). Mechanism and optimization of a graphene/silicon hybrid diode terahertz modulator. ACS Appl. Electron. Mater. ***2***: 1953–1959.
43. Wei, M., Zhang, D., Zhang, L., et al. (2021). High-performance multifunctional photodetector and THz modulator based on graphene/TiO_2/p-Si heterojunction. Nanoscale Res. Lett. ***16***: 134.
44. Roy, K., Padmanabhan, M., Goswami, S., et al. (2013). Graphene–MoS_2 hybrid structures for multifunctional photoresponsive memory devices. Nat. Nanotechnol. ***8***: 826–830.
45. Li, X., Zhu, H., Wang, K., et al. (2010). Graphene-on-silicon Schottky junction solar cells. Adv. Mater. ***22***: 2743–2748.
46. Li, X., Xie, D., Park, H., et al. (2013). Ion doping of graphene for high-efficiency heterojunction solar cells. Nanoscale ***5***: 1945–1948.
47. Liu, X., Zhang, X.W., Yin, Z.G., et al. (2014). Enhanced efficiency of graphene-silicon Schottky junction solar cells by doping with Au nanoparticles. Appl. Phys. Lett. ***105***: 183901. https://doi.org/10.1063/1.4901106.
48. Che, S., Jasuja, K., Behura, S.K., et al. (2017). Retained carrier-mobility and enhanced plasmonic-photovoltaics of graphene via ring-centered η^6 functionalization and nanointerfacing. Nano Lett. ***17***: 4381–4389.
49. Shi, E., Li, H., Yang, L., et al. (2013). Colloidal antireflection coating improves graphene–silicon solar cells. Nano Lett. ***13***: 1776–1781.
50. Meng, J.H., Liu, X., Zhang, X.W., et al. (2016). Interface engineering for highly efficient graphene-on-silicon Schottky junction solar cells by introducing a hexagonal boron nitride interlayer. Nano Energy ***28***: 44–50.
51. Song, Y., Li, X., Mackin, C., et al. (2015). Role of interfacial oxide in high-efficiency graphene–silicon Schottky barrier solar cells. Nano Lett. ***15***: 2104–2110.
52. Xu, D., He, J., Yu, X., et al. (2017). Illumination-induced hole doping for performance improvement of graphene/n-silicon solar cells with P_3HT interlayer. Adv. Electron. Mater. ***3***: 1600516. https://doi.org/10.1002/aelm.201600516.
53. Jiao, K., Duan, C., Wu, X., et al. (2015). The role of MoS_2 as an interfacial layer in graphene/silicon solar cells. Phys. Chem. Chem. Phys. ***17***: 8182–8186.
54. Tsuboi, Y., Wang, F., Kozawa, D., et al. (2015). Enhanced photovoltaic performances of graphene/Si solar cells by insertion of a MoS_2 thin film. Nanoscale ***7***: 14476–14482.
55. Song, Y., Osherov, A., Bulović, V., et al. (2018). Graphene–perovskite Schottky barrier solar cells. Adv. Sustain. Syst. ***2***: 1700106. https://doi.org/10.1002/adsu.201700106.
56. Agresti, A., Pescetelli, S., Palma, A.L., et al. (2017). Graphene interface engineering for perovskite solar modules: 12.6% power conversion efficiency over 50 cm^2 active area. ACS Energy Lett. ***2***: 279–287.
57. Lang, F., Gluba, M.A., Albrecht, S., et al. (2015). Perovskite solar cells with large-area CVD-graphene for tandem solar cells. J. Phys. Chem. Lett. ***6***: 2745–2750.
58. Lin, S.S., Wu, Z.Q., Li, X.Q., et al. (2016). Stable 16.2% efficient surface plasmon-enhanced graphene/GaAs heterostructure solar cell. Adv. Energy Mater. ***6***: 1600822. https://doi.org/10.1002/aenm.201600822.
59. Wang, P., Li, X., Xu, Z., et al. (2015). Tunable graphene/indium phosphide heterostructure solar cells. Nano Energy ***13***: 509–517.
60. Li, X., Chen, W., Zhang, S., et al. (2015). 18.5% efficient graphene/GaAs van der Waals heterostructure solar cell. Nano Energy ***16***: 310–319.
61. Agresti, A., Pescetelli, S., Taheri, B., et al. (2016). Graphene–perovskite solar cells exceed 18% efficiency: a stability study. ChemSusChem ***9***: 2609–2619.
62. Xiang, Q., Yu, J., and Jaroniec, M. (2012). Graphene-based semiconductor photocatalysts. Chem. Soc. Rev. ***41***: 782–796.
63. Zhu, Z.Y., Cheng, Y.C., and Schwingenschlögl, U. (2011). Giant spin-orbit-induced spin splitting in two-dimensional transition-metal dichalcogenide semiconductors. Phys. Rev. B ***84***: 153402. https://doi.org/10.1103/PhysRevB.84.153402.
64. Liu, M., Yin, X., Ulin-Avila, E., et al. (2011). A graphene-based broadband optical modulator. Nature ***474***: 64–67.
65. Phare, C.T., Daniel Lee, Y.H., Cardenas, J., et al. (2015). Graphene electro-optic modulator with 30 GHz bandwidth. Nat. Photonics ***9***: 511–514.
66. Zhou, H., Chen, Y., and Zhu, H. (2021). Deciphering asymmetric charge transfer at transition metal dichalcogenide-graphene interface by helicity-resolved ultrafast spectroscopy. Sci. Adv. ***7***: eabg2999. https://doi.org/10.1126/sciadv.abg2999.
67. Hill, H.M., Rigosi, A.F., Raja, A., et al. (2017). Exciton broadening in WS_2/graphene heterostructures. Phys. Rev. B ***96***: 205401. https://doi.org/10.1103/PhysRevB.96.205401.
68. Aeschlimann, S., Rossi, A., Chávez-Cervantes, M., et al. (2020). Direct evidence for efficient ultrafast charge separation in epitaxial WS_2/graphene heterostructures. Sci. Adv. ***6***: eaay0761. https://doi.org/10.1126/sciadv.aay0761.
69. Trovatello, C., Piccinini, G., Forti, S., et al. (2022). Ultrafast hot carrier transfer in WS_2/graphene large area heterostructures. NPJ 2D Mater. Appl. ***6***: 24.
70. Yuan, L., Chung, T.F., Kuc, A., et al. (2018). Photocarrier generation from interlayer charge-transfer transitions in WS_2-graphene heterostructures. Sci. Adv. ***4***: e1700324. https://doi.org/10.1126/sciadv.1700324.
71. Liu, X., Pei, J., Hu, Z., et al. (2020). Manipulating charge and energy transfer between 2D atomic layers via heterostructure engineering. Nano Lett. ***20***: 5359–5366.
72. Ahmed, T., Roy, K., Kakkar, S., et al. (2020). Interplay of charge transfer and disorder in optoelectronic response in Graphene/hBN/MoS_2 van der Waals heterostructures. 2D Mater. ***7***: 025043. https://doi.org/10.1088/2053-1583/ab771f.
73. Luo, D., Tang, J., Shen, X., et al. (2021). Twist-angle-dependent ultrafast charge transfer in MoS_2-graphene van der Waals heterostructures. Nano Lett. ***21***: 8051–8057.
74. Froehlicher, G., Lorchat, E., and Berciaud, S. (2018). Charge versus energy transfer in atomically thin graphene-transition metal dichalcogenide van der Waals heterostructures. Phys. Rev. X ***8***: 011007. https://doi.org/10.1103/PhysRevX.8.011007.
75. Fu, S., Jia, X., Hassan, A.S., et al. (2023). Reversible electrical control of interfacial charge flow across van der Waals interfaces. Nano Lett. ***23***: 1850–1857.
76. Yu, X., Fu, S., Mandal, M., et al. (2022). Tuning interfacial charge transfer in atomically precise nanographene–graphene heterostructures by engineering van der Waals interactions. J. Chem. Phys. ***156***: 074702. https://doi.org/10.1063/5.0081074.
77. Zhang, H., Debroye, E., Fu, S., et al. (2023). Optical switching of hole transfer in double-perovskite/graphene heterostructure. Adv. Mater. ***35***: 2211198. https://doi.org/10.1002/adma.202211198.
78. Jnawali, G., Rao, Y., Beck, J.H., et al. (2015). Observation of ground- and excited-state charge transfer at the C_{60}/graphene interface. ACS Nano ***9***: 7175–7185.
79. Dong, S., Beaulieu, S., Selig, M., et al. (2023). Observation of ultrafast interfacial Meitner-Auger energy transfer in a van der Waals heterostructure. Nat. Commun. ***14***: 5057.
80. Krause, R., Chávez-Cervantes, M., Aeschlimann, S., et al. (2021). Ultrafast charge separation in bilayer WS_2/graphene heterostructure revealed by time-and angle-resolved photoemission spectroscopy. Front. Phys. ***9***: 668149. https://doi.org/10.3389/fphy.2021.668149.
81. Hofmann, N., Weigl, L., Gradl, J., et al. (2023). Link between interlayer hybridization and ultrafast charge transfer in WS_2-graphene heterostructures. 2D Mater. ***10***: 035025. https://doi.org/10.1088/2053-1583/acdaab.
82. Chen, Z., Berciaud, S., Nuckolls, C., et al. (2010). Energy transfer from individual semiconductor nanocrystals to graphene. ACS Nano ***4***: 2964–2968.
83. Krause, R., Aeschlimann, S., Chávez-Cervantes, M., et al. (2021). Microscopic understanding of ultrafast charge transfer in van der Waals heterostructures. Phys. Rev. Lett. ***127***: 276401. https://doi.org/10.1103/PhysRevLett.127.276401.
84. Hu, Z., Liu, X., Hernández-Martínez, P.L., et al. (2022). Interfacial charge and energy transfer in van der Waals heterojunctions. InfoMat ***4***: e12290. https://doi.org/10.1002/inf2.12290.
85. Bradac, C., Xu, Z.Q., and Aharonovich, I. (2021). Quantum energy and charge transfer at two-dimensional interfaces. Nano Lett. ***21***: 1193–1204.
86. Brédas, J.L., Beljonne, D., Coropceanu, V., et al. (2004). Charge-transfer and energy-transfer processes in π-conjugated oligomers and polymers: a molecular picture. Chem. Rev. ***104***: 4971–5004.
87. Ho, C.L., and Wong, W.Y. (2013). Charge and energy transfers in functional metallophosphors and metallopolyynes. Coord. Chem. Rev. ***257***: 1614–1649.
88. May, V., and Kühn, O. (2023). Charge and Energy Transfer Dynamics in Molecular Systems (John Wiley & Sons). https://doi.org/10.1002/9783527633791.
89. Clegg, R.M. (1995). Fluorescence resonance energy transfer. Curr. Opin. Biotechnol. ***6***: 103–110.
90. Swathi, R.S., and Sebastian, K.L. (2009). Long range resonance energy transfer from a dye molecule to graphene has $(distance)^{-4}$ dependence. J. Chem. Phys. ***130***: 086101. https://doi.org/10.1063/1.3077292.
91. Gaudreau, L., Tielrooij, K.J., Prawiroatmodjo, G.E.D.K., et al. (2013). Universal distance-scaling of nonradiative energy transfer to graphene. Nano Lett. ***13***: 2030–2035.
92. Moore, J.H. (1973). Investigation of the Wigner spin rule in collisions of N^+ with He, Ne, Ar, N_2, and O_2. Phys. Rev. A ***8***: 2359–2362.
93. Tielrooij, K.J., Hesp, N.C.H., Principi, A., et al. (2018). Out-of-plane heat transfer in van der Waals stacks through electron–hyperbolic phonon coupling. Nat. Nanotechnol. ***13***: 41–46.
94. Cano, D., Ferrier, A., Soundarapandian, K., et al. (2020). Fast electrical modulation of strong near-field interactions between erbium emitters and graphene. Nat. Commun. ***11***: 4094.
95. Fang, H., and Hu, W. (2017). Photogating in low dimensional photodetectors. Adv. Sci. ***4***: 1700323. https://doi.org/10.1002/advs.201700323.
96. Tan, H., Fan, Y., Zhou, Y., et al. (2016). Ultrathin 2D photodetectors utilizing chemical vapor deposition grown WS_2 with graphene electrodes. ACS Nano ***10***: 7866–7873.
97. Mehew, J.D., Unal, S., Torres Alonso, E., et al. (2017). Fast and highly sensitive ionic-polymer-gated WS_2–graphene photodetectors. Adv. Mater. ***29***: 1700222. https://doi.org/10.1002/adma.201700222.
98. Chen, T., Sheng, Y., Zhou, Y., et al. (2019). High photoresponsivity in ultrathin 2D lateral graphene:WS_2:graphene photodetectors using direct CVD growth. ACS Appl. Mater. Interfaces ***11***: 6421–6430.
99. Brenneis, A., Gaudreau, L., Seifert, M., et al. (2015). Ultrafast electronic readout of diamond nitrogen–vacancy centres coupled to graphene. Nat. Nanotechnol. ***10***: 135–139.
100. Ulstrup, S., Čabo, A.G., Miwa, J.A., et al. (2016). Ultrafast band structure control of a two-dimensional heterostructure. ACS Nano ***10***: 6315–6322.
101. Ferrante, C., Di Battista, G., López, L.E.P., et al. (2022). Picosecond energy transfer in a transition metal dichalcogenide–graphene heterostructure revealed by transient Raman spectroscopy. Proc. Natl. Acad. Sci. USA ***119***: e2119726119. https://doi.org/10.1073/pnas.2119726119.

102. Ferrante, C., Virga, A., Benfatto, L., et al. (2018). Raman spectroscopy of graphene under ultrafast laser excitation. Nat. Commun. ***9***: 308.
103. Bruna, M., Ott, A.K., Ijäs, M., et al. (2014). Doping dependence of the Raman spectrum of defected graphene. ACS Nano ***8***: 7432–7441.
104. Lee, J.E., Ahn, G., Shim, J., et al. (2012). Optical separation of mechanical strain from charge doping in graphene. Nat. Commun. ***3***: 1024.
105. Yan, J., Zhang, Y., Kim, P., et al. (2007). Electric field effect tuning of electron-phonon coupling in graphene. Phys. Rev. Lett. ***98***: 166802. https://doi.org/10.1103/PhysRevLett.98.166802.
106. Ferrari, A.C., and Basko, D.M. (2013). Raman spectroscopy as a versatile tool for studying the properties of graphene. Nat. Nanotechnol. ***8***: 235–246.
107. Berciaud, S., Han, M.Y., Mak, K.F., et al. (2010). Electron and optical phonon temperatures in electrically biased graphene. Phys. Rev. Lett. ***104***: 227401. https://doi.org/10.1103/PhysRevLett.104.227401.
108. Selig, M., Malic, E., Ahn, K.J., et al. (2019). Theory of optically induced Förster coupling in van der Waals coupled heterostructures. Phys. Rev. B ***99***: 035420. https://doi.org/10.1103/PhysRevB.99.035420.
109. Zhou, H., Chen, Y., and Zhu, H. (2024). Harnessing hot carriers in two-dimensional materials. J. Phys. Chem. C ***128***: 9828–9836.
110. Chen, Y., Sun, C., Zhou, H., et al. (2021). Controlling photocarrier lifetime in graphene for enhanced photocurrent generation via cascade hot electron transfer. J. Phys. Chem. Lett. ***12***: 9989–9994.
111. Wen, G., Fu, S., Bonn, M., et al. (2024). Compositional engineering of interfacial charge transfer in van der Waals heterostructures of graphene and transition metal dichalcogenides. J. Chem. Phys. ***161***: 054714. https://doi.org/10.1063/5.0210906.
112. Lin, Y., Ma, Q., Shen, P.C., et al. (2019). Asymmetric hot-carrier thermalization and broadband photoresponse in graphene-2D semiconductor lateral heterojunctions. Sci. Adv. ***5***: eaav1493. https://doi.org/10.1126/sciadv.aav1493.
113. Massicotte, M., Schmidt, P., Vialla, F., et al. (2016). Photo-thermionic effect in vertical graphene heterostructures. Nat. Commun. ***7***: 12174. https://doi.org/10.1038/ncomms12174.
114. Paul, K.K., Kim, J.H., and Lee, Y.H. (2021). Hot carrier photovoltaics in van der Waals heterostructures. Nat. Rev. Phys. ***3***: 178–192.
115. Liu, C., Lu, Y., Shen, R., et al. (2022). Dynamics and physical process of hot carriers in optoelectronic devices. Nano Energy ***95***: 106977. https://doi.org/10.1016/j.nanoen.2022.106977.
116. Ding, Y.T., Zhang, B.Y., Sun, C.L., et al. (2023). Optoelectronic materials utilizing hot excitons or hot carriers: from mechanism to applications. J. Mater. Chem. C ***11***: 7937–7956.
117. Ahmed, I., Shi, L., Pasanen, H., et al. (2021). There is plenty of room at the top: generation of hot charge carriers and their applications in perovskite and other semiconductor-based optoelectronic devices. Light Sci. Appl. ***10***: 174.
118. Chen, Y., Li, Y., Zhao, Y., et al. (2019). Highly efficient hot electron harvesting from graphene before electron-hole thermalization. Sci. Adv. ***5***: eaax9958. https://doi.org/10.1126/sciadv.aax9958.
119. Winzer, T., Knorr, A., and Malic, E. (2010). Carrier multiplication in graphene. Nano Lett. ***10***: 4839–4843.
120. Tomadin, A., Hornett, S.M., Wang, H.I., et al. (2018). The ultrafast dynamics and conductivity of photoexcited graphene at different Fermi energies. Sci. Adv. ***4***: eaar5313. https://doi.org/10.1126/sciadv.aar5313.
121. Gabor, N.M., Song, J.C.W., Ma, Q., et al. (2011). Hot carrier–assisted intrinsic photoresponse in graphene. Science ***334***: 648–652.
122. Ma, Q., Andersen, T.I., Nair, N.L., et al. (2016). Tuning ultrafast electron thermalization pathways in a van der Waals heterostructure. Nat. Phys. ***12***: 455–459.
123. Ulbricht, R., Hendry, E., Shan, J., et al. (2011). Carrier dynamics in semiconductors studied with time-resolved terahertz spectroscopy. Rev. Mod. Phys. ***83***: 543–586.
124. Shi, S.F., Tang, T.T., Zeng, B., et al. (2014). Controlling graphene ultrafast hot carrier response from metal-like to semiconductor-like by electrostatic gating. Nano Lett. ***14***: 1578–1582.
125. Frenzel, A.J., Lui, C.H., Shin, Y.C., et al. (2014). Semiconducting-to-metallic photoconductivity crossover and temperature-dependent Drude weight in graphene. Phys. Rev. Lett. ***113***: 056602. https://doi.org/10.1103/PhysRevLett.113.056602.
126. Jensen, S.A., Mics, Z., Ivanov, I., et al. (2014). Competing ultrafast energy relaxation pathways in photoexcited graphene. Nano Lett. ***14***: 5839–5845.
127. Jnawali, G., Rao, Y., Yan, H., et al. (2013). Observation of a transient decrease in terahertz conductivity of single-layer graphene induced by ultrafast optical excitation. Nano Lett. ***13***: 524–530.
128. Wang, S., Xie, Z., Zhu, D., et al. (2023). Efficient photocatalytic production of hydrogen peroxide using dispersible and photoactive porous polymers. Nat. Commun. ***14***: 6891.
129. Maji, T.K., Bagchi, D., Kar, P., et al. (2017). Enhanced charge separation through modulation of defect-state in wide band-gap semiconductor for potential photocatalysis application: ultrafast spectroscopy and computational studies. J. Photochem. Photobiol. Chem. ***332***: 391–398.
130. Chen, R., Pang, S., An, H., et al. (2019). Giant defect-induced effects on nanoscale charge separation in semiconductor photocatalysts. Nano Lett. ***19***: 426–432.
131. Hamed, A., Sun, Y.Y., Tao, Y.K., et al. (1993). Effects of oxygen and illumination on the in situ conductivity of C_{60} thin films. Phys. Rev. B ***47***: 10873–10880.
132. Lee, C.H., Yu, G., Kraabel, B., et al. (1994). Effects of oxygen on the photocarrier dynamics in a C_{60} film: Studies of transient and steady-state photoconductivity. Phys. Rev. B ***49***: 10572–10576.
133. Schuler, B., Qiu, D.Y., Refaely-Abramson, S., et al. (2019). Large spin-orbit splitting of deep in-gap defect states of engineered sulfur vacancies in monolayer WS_2. Phys. Rev. Lett. ***123***: 76801. https://doi.org/10.1103/PhysRevLett.123.076801.
134. Gali, S.M., and Beljonne, D. (2021). Combined healing and doping of transition metal dichalcogenides through molecular functionalization. J. Mater. Chem. C ***9***: 16247–16256.
135. Park, T.G., Choi, B.K., Park, J., et al. (2021). Interlayer coupling and ultrafast hot electron transfer dynamics in metallic VSe_2/graphene van der Waals heterostructures. ACS Nano ***15***: 7756–7764.
136. Gobre, V.V., and Tkatchenko, A. (2013). Scaling laws for van der Waals interactions in nanostructured materials. Nat. Commun. ***4***: 2341.
137. Hong, J., Hu, Z., Probert, M., et al. (2015). Exploring atomic defects in molybdenum disulphide monolayers. Nat. Commun. ***6***: 6293.
138. Handa, T., Holbrook, M., Olsen, N., et al. (2024). Spontaneous exciton dissociation in transition metal dichalcogenide monolayers. Sci. Adv. ***10***: eadj4060. https://doi.org/10.1126/sciadv.adj4060.
139. Liu, Y., Liu, H., Wang, J., et al. (2022). Defect-type-dependent carrier lifetimes in monolayer WS_2 films. J. Phys. Chem. C ***126***: 4929–4938.
140. Shin, D., Wang, G., Han, M., et al. (2021). Preferential hole defect formation in monolayer WSe_2 by electron-beam irradiation. Phys. Rev. Mater. ***5***: 044002. https://doi.org/10.1103/PhysRevMaterials.5.044002.
141. Bretscher, H., Li, Z., Xiao, J., et al. (2021). Rational passivation of sulfur vacancy defects in two-dimensional transition metal dichalcogenides. ACS Nano ***15***: 8780–8789.
142. Wang, C., Chen, Y., Ma, Q., et al. (2024). Revealing the fundamental limit of gate-controlled ultrafast charge transfer in graphene–MoS_2 heterostructures. ACS Photonics ***11***: 5170–5179. https://doi.org/10.1021/acsphotonics.4c01391.
143. Wang, C., Chen, Y., Ma, Q., et al. (2024). Observation of transient trion induced by ultrafast charge transfer in graphene/MoS_2 heterostructure. Preprint at: arXiv. 2409.17752. https://doi.org/10.48550/arXiv.2409.17752
144. Nguyen, N.N., Lee, H., Lee, H.C., et al. (2022). Van der Waals epitaxy of organic semiconductor thin films on atomically thin graphene templates for optoelectronic applications. Acc. Chem. Res. ***55***: 673–684.
145. Xiong, Y., Liao, Q., Huang, Z., et al. (2020). Ultrahigh responsivity photodetectors of 2D covalent organic frameworks integrated on graphene. Adv. Mater. ***32***: 1907242. https://doi.org/10.1002/adma.201907242.
146. Han, J., Feng, J., Kang, J., et al. (2024). Fast growth of single-crystal covalent organic frameworks for laboratory x-ray diffraction. Science ***383***: 1014–1019.
147. Wang, Z., Fu, S., Zhang, W., et al. (2024). A Cu_3BHT-graphene van der Waals heterostructure with strong interlayer coupling for highly efficient photoinduced charge separation. Adv. Mater. ***36***: 2311454. https://doi.org/10.1002/adma.202311454.
148. Liu, J., Chen, Y., Huang, X., et al. (2024). On-liquid-gallium surface synthesis of ultrasmooth thin films of conductive metal–organic frameworks. Nat. Synth. ***3***: 715–726.
149. Lu, A.Y., Zhu, H., Xiao, J., et al. (2017). Janus monolayers of transition metal dichalcogenides. Nat. Nanotechnol. ***12***: 744–749.
150. Liu, X., Gao, P., Hu, W., et al. (2020). Photogenerated-carrier separation and transfer in two-dimensional Janus transition metal dichalcogenides and graphene van der Waals sandwich heterojunction photovoltaic cells. J. Phys. Chem. Lett. ***11***: 4070–4079.
151. Garcia, J.H., Vila, M., Cummings, A.W., et al. (2018). Spin transport in graphene/transition metal dichalcogenide heterostructures. Chem. Soc. Rev. ***47***: 3359–3379. https://doi.org/10.1039/C7CS00864C.
152. Drögeler, M., Franzen, C., Volmer, F., et al. (2016). Spin lifetimes exceeding 12 ns in graphene nonlocal spin valve devices. Nano Lett. ***16***: 3533–3539.
153. Ingla-Aynés, J., Meijerink, R.J., and Wees, B.J. (2016). Eighty-eight percent directional guiding of spin currents with 90 μm relaxation length in bilayer graphene using carrier drift. Nano Lett. ***16***: 4825–4830.
154. He, J., Li, S., Bandyopadhyay, A., et al. (2021). Unravelling photoinduced interlayer spin transfer dynamics in two-dimensional nonmagnetic-ferromagnetic van der Waals heterostructures. Nano Lett. ***21***: 3237–3244.

ACKNOWLEDGMENTS

K.-J.T. acknowledges funding from European Union's Horizon 2020 Research and Innovation Programme under grant agreement no. 804349 (ERC StG CUHL) and FLAG-ERA grant ENPHOCAL, by MICIN with no. PCI2021-122101-2A (Spain). ICN2 was supported by the Severo Ochoa program from Spanish MINECO grant no. SEV-2017-0706. The funders had no role in the study design, data collection and analysis, decision to publish, or preparation of the manuscript. H.I.W's website is https://sites.google.com/view/hai-wang-at-mpip and M.B.'s website is https://www.mpip-mainz.mpg.de/en/bonn.

AUTHOR CONTRIBUTIONS

M.B. and H.I.W. conceived and supervised this article. S.F., H.Z., and H.I.W. drafted the article, which was revised and commented on by all authors. All authors contributed to the manuscript and approved the final version.

DECLARATION OF INTERESTS

The authors declare no competing interests.

LEAD CONTACT WEBSITE

The lead contact's website is at https://www.mpip-mainz.mpg.de/en/bonn.